Eur. Phys. J. Plus (2024) 139:884
https://doi.org/10.1140/epjp/s13360-024-05664-4

THE EUROPEAN PHYSICAL JOURNAL PLUS

Review

Prompt-gamma imaging in particle therapy

Marco Pinto[a]

Department of Experimental Physics - Medical Physics, Ludwig-Maximilians-Universität (LMU) München, Garching bei München, Germany

Received: 19 February 2024 / Accepted: 14 September 2024

Abstract Prompt-gamma imaging has been a source of intensive research over the years since its first proposal in 2003. Several detection approaches have been researched and developed, and many studies on prompt-gamma imaging have been conducted on its feasibility, detection systems optimisation, and possible workflows. Now, this form of particle therapy monitoring is finally arriving in clinical settings and showing impressive results. Prompt-gamma imaging may be the key to enabling crucial improvements in particle therapy, namely when considering more complex workflow scenarios, like adaptive radiotherapy using ion beams. Herein, several aspects related to prompt-gamma imaging are introduced, covering both its advantages and limitations. The need for particle therapy monitoring, the different prompt-gamma radiation detection systems, the difficulties with dealing with low emission yields and with the tools used to simulate it, the prediction tools for prompt-gamma radiation, and the translation into clinical applications are presented and discussed. Finally, some considerations are also made on the future of prompt-gamma imaging and what it may bring into particle therapy, ultimately benefiting patients worldwide.

1 Introduction

Ions are known for their superior ballistic properties compared to photons [4, 62, 100], which gives particle therapy better tumour conformity when compared to photon radiotherapy for the same number of beams. Furthermore, higher tumour conformity and fewer beams lead to a lower total dose delivered to the healthy tissues [23]. However, the same physics processes that make particle therapy advantageous from a ballistic point of view also make particle therapy more susceptible to range uncertainties [57, 61].

Prompt-gamma imaging was proposed in the year of 2003 in a submission to the 39th Particle Therapy Co-Operative Group (PTCOG) Conference by Jongen and Stichelbaut entitled "Verification of the proton beam position in the patient by the prompt gamma rays emission". The words written back then still resonate today, and it is good to remember them [53]:

> "Several authors have studied the production of PET isotopes by therapeutic proton beams. The goal is to use a PET scanner to verify the location of the proton beam in the patient body immediately after the treatment. But, when protons are stopped in the patient body, they produce also copious amounts of prompt gamma rays, which could be imaged during the irradiation using a classical gamma camera. This would allow visualizing the proton energy deposition in the patient. We have conducted Monte Carlo simulations of this problem using the GEANT Code. These simulations indicate that this method could offer a real potential in proton therapy treatment quality assurance."

Since that first proposal, the field has evolved considerably regarding competing approaches but always with the same goal of obtaining indirect information about ion ranges and thus improving the quality assurance (QA) of particle therapy treatments. Nevertheless, many challenges and open questions remain, especially concerning clinical implementation and workflow. These headwinds have translated into a poor adoption of this form of treatment monitoring so far.

This paper aims to give an overall view of the prompt-gamma (PG) imaging field, how we arrived here and some hints of where it may be headed. Several aspects described and discussed herein apply to particle therapy as a whole, but most of the content focuses on proton therapy. The research and developments of PG imaging in the context of proton therapy are more mature than in other types of particle therapy, for example, carbon ion therapy.

2 The need for particle therapy monitoring

Theoretically, ions allow for precise local dose deposition with their characteristic depth-dose curve (Bragg curve) and its Bragg peak. However, the finite range of ions in matter and the underlying physics processes make particle therapy more prone to a mismatch

[a] e-mail: Marco.Pinto@physik.uni-muenchen.de (corresponding author)

Published online: 09 October 2024

between the intended and delivered dose distribution. This possibility of mismatch brings the concept of range uncertainties [57, 65, 102]. In his review paper in 2012, Paganetti [102] listed the sources of range uncertainties as imaging, patient setup, beam delivery and dose calculation. The clinical approach to dealing with these uncertainties has been adding margins at the treatment planning phase that can ideally enclose such range deviations, ensuring proper dose delivery to the target volumes. The choice of margins differs among clinical facilities, and it is typically presented as a proton range-dependent margin plus an absolute margin. Even though cautioning for possible larger margins in specific treatment scenarios, Paganetti [102] presented proton range-dependent margins ranging from 2.5% up to 4.6% and absolute margins in the range of 1.0 to 3.0 mm. Tattenberg *et al*. [158] approximate the clinical margins to a single proton range-dependent component of 4%. This value of 4% translates into an additional margin of 8 mm, considering a proton range of 20 cm. Additional margins affect the clinical exploitation of the ballistic advantages provided by ions by unnecessarily irradiating healthy tissues, which can lead to increased toxicity effects [126, 148].

Range uncertainties can also be tackled by asserting plan robustness. For example, the work of Unkelbach *et al*. [168] proposes a method for treatment plan optimisation based on the worst-case dose distribution by assuming that the proton range may vary within some interval. Pflugfelder *et al*. [115] extended the work of Unkelbach *et al*. to allow any objective function in the worst-case optimisation and by including the possibility of setup uncertainties. Chen *et al*. [20] developed a multi-criteria optimisation framework in which the optimisation is performed under several robustness criteria. Finally, in this list of examples, it is noteworthy to include the work of Souris *et al*. [152], where the authors conceived a Monte Carlo approach in which systematic and random errors are randomly sampled from possible scenarios based on 4D imaging data. Such an approach allows for a comprehensive Monte Carlo simulation of setup and range errors, variation of the breathing motion, and interplay effect.

The issue of range uncertainties is not limited to the effects of adding margins. The uncertainty on the position of the Bragg peak and, consequently, the possibility of overshooting into an organ-at-risk (OAR) located in the proximity of the target volumes created the clinical practice of avoiding the position of an OAR immediately after the distal edge of the ion beam. This constraint in the beam angle arrangements can have a detrimental impact on the quality of the treatment when compared to alternatives without such a constraint. A clear example is the prostate proton treatment. Unless the patient has undergone hip replacement, current clinical practice generally uses lateral fields so that OARs in this anatomical region can be spared. However, this beam arrangement exhibits poorer quality in several dosimetric quantities than the alternative anterior-oblique beams [97, 157]. The arrangement with lateral fields is not necessarily an inferior solution since it ultimately depends from case to case. The concern is that anterior-oblique beams cannot often be considered due to range uncertainties.

Regardless of the impact of range uncertainties on the overall quality of a particle therapy treatment, it is essential to mention that some authors see their magnitude and consequences as sometimes misunderstood and overestimated when dealing with clinical applications [78]. Careful selection of the beam angle arrangements can avoid many situations where OARs are close to the distal edge, and the critical structures can then be spared using the lateral edges, which are usually less sharp than the distal one [57, 78]. If Bragg peaks are obtained in water, the distal edge fall-off is indeed steep and justifies much of the concerns regarding the potential impact of misplacing it in the patient. However, the patient heterogeneities can have a striking effect on the dose distributions, thus blurring the distal edge [78]. The example shown in [78] depicts a clinical case where the lateral fall-off is sharper than the distal one. These views do not downplay range uncertainties, nor that they should not be considered. Understanding that current practice has tools and approaches that can minimise their effects is essential. On the other hand, the issues posed by range uncertainties may increase when trying to improve the status quo in the field. Approaches like adaptive radiotherapy or hypofractionation schemes are two examples that could greatly benefit from the mitigation of range uncertainties.

3 Secondary-radiation monitoring and PG emission

A possible approach to tackle range uncertainties is to employ some form of treatment monitoring relying on secondary radiation that can escape the patient and be detected. Hereafter, only the term treatment monitoring will be used to refer to the monitoring form mentioned above. Other methods do exist, for example, rectal balloons with detectors [19, 42], MR imaging [33, 57, 183] or ionoacoustics [7, 18]. Treatment monitoring techniques do not reduce range uncertainties since these uncertainties are linked to imaging used for planning, patient setup, beam delivery and dose calculation [102]. This reality contrasts with other strategies like the usage of Monte Carlo tools for dose calculation [102] or ion imaging for planning [27], which can effectively reduce range uncertainties. Treatment monitoring gives, with some uncertainty dependent on statistics and technique, an assessment of the quality of the treatment delivered.

Secondary radiation can be created via electromagnetic or nuclear interactions. The former is the basis of secondary-electron-bremsstrahlung (SEB) imaging, which is a technique that detects the photons escaping the patient after being created by the bremsstrahlung of secondary electrons [179, 180]. It is not yet used in clinical applications, but it has been experimentally demonstrated for both proton [179] and carbon ion [180] beams. Nuclear interactions produce a wealth of secondary radiation and radionuclides that can be used for treatment monitoring. Figure 1 shows a sketch of possible nuclear interactions in particle therapy.

Regarding radionuclides, we are specifically interested in positron-emitting radionuclides, where the two annihilation photons can be detected after positron emission and consequent electron-positron annihilation. Such a technique gives rise to positron emission tomography (PET) monitoring, the first approach routinely employed in a clinical setting [13, 103, 108–110]. Due to the nature of

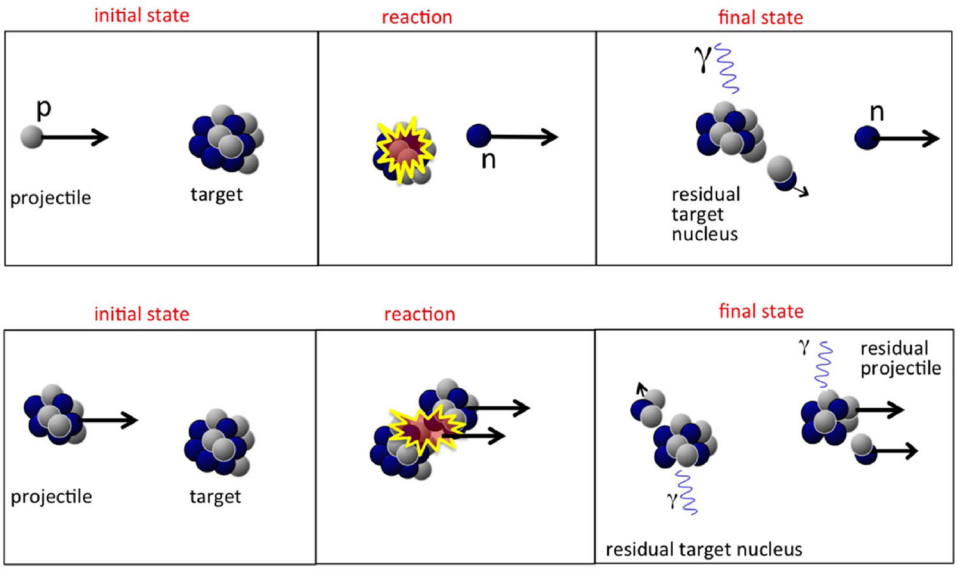

Fig. 1 Top: sketch of a possible nucleon-nucleus reaction in proton therapy, whereby a neutron and a photon are created. Bottom: sketch of nucleus-nucleus reaction in heavy ion therapy with creation of light fragments and photons. Reproduced from [61] under the terms of the Creative Commons Attribution License (CC BY, https://creativecommons.org/licenses/by/4.0/)

using delayed radiation, PET monitoring has specificities regarding detection, namely the detection time frame (in-beam, in-room and offline [147]) and washout [5, 37, 95], the physiological process that removes positron-emitting radionuclides from the place of creation. Exploring PET monitoring is outside of the scope of this manuscript. However, it is essential to highlight how important the experience and lessons obtained in that context shape the entire field of treatment monitoring.

Another form of secondary-radiation monitoring built on top of nuclear interactions is interaction vertex imaging (IVI) [38, 47, 98]. In this case, the aim is to detect secondary protons escaping the patient and to reconstruct the vertex position of said secondary protons. Light fragments may also escape and be detected, but their fraction is tiny in comparison to secondary protons [139]. This method can only be used when delivering heavier ions since it relies on creating secondary protons that can escape the patient. IVI has been primarily researched in the context of carbon ion therapy.

When excited nuclei created in nuclear interactions release excess energy, PG radiation may be emitted. For practical purposes in particle therapy, PG emission occurs where nuclear interaction happens since PG radiation is emitted almost instantly. Thus, the emission distribution is not affected by any physiological process (washout) nor by physical processes that may interfere with determining the location of the nuclear interaction, for example, the positron path before electron-positron annihilation. Figure 2 depicts the stages of a nuclear interaction between a proton and a target nucleus in the energy range relevant to proton therapy. The PG radiation energy spectrum is characterized by the continuum and the discrete components. The origin of prompt gammas was eloquently summarized by Le Fouhler *et al*. [69] and reproduced here: *"the continuum energy spectrum can be divided into three components. High energy gamma-rays (E > 30 MeV) are mainly produced during nucleon-nucleon bremsstrahlung at the very beginning of the reaction. Between 10 and 30 MeV, prompt-gamma rays are emitted during the decay of giant resonances, mostly Giant Dipole Resonances (GDR), a collective oscillation between protons and neutrons in the nucleus. Below 10 MeV, the main contribution for gamma production is statistical photons coming from the remaining excited fragments at the final stage of the reaction. Lastly, at the end of the evaporation cascade, photons with discrete energies are emitted. The prompt-gamma ray spectrum is dominated by statistical photons whose energy ranges from a few keV up to 10–15 MeV"* [69]. The discrete, or characteristic, emission is particularly interesting because it can be associated with specific target nuclei, and its yield can be estimated using proton energy. These features offer the possibility of extracting relevant PG-related information for monitoring purposes, which will be covered later. In Verburg *et al*. , one can find a table with a comprehensive compilation of the most important characteristic emissions in proton therapy [170].

As nuclear interactions ensue almost all along the entire path of the beam, it allows for monitoring the range of its particles, assuming that the nuclear interactions can be correlated with the energy deposition behaviour along the beam path, namely around the end of the particle range. PG emission can happen with incident proton energies of a few MeV [170] for typical target nuclei in a patient body, which puts the location of the end of the PG emission very close to the end of the proton range. A comparison of dose and PG distributions can be observed in Fig. 3. This figure was obtained with Monte Carlo (MC) simulations using two computed tomography (CT) datasets of the same patient but taken at different times during a radiotherapy treatment. It mimics a relevant clinical scenario where anatomical changes occur and the resulting impact on dose and PG distributions.

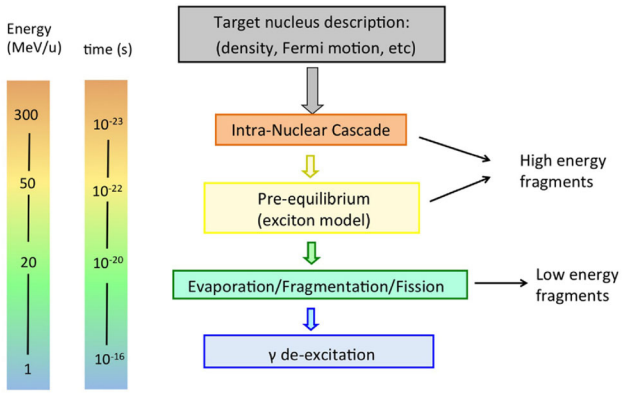

Fig. 2 Schematic showing the stages in a nuclear interaction between a proton and a target nucleus in the energy range relevant to proton therapy. The time scale of the different steps and energy of the interacting particle are also displayed. Reproduced from [61] under the terms of the Creative Commons Attribution License (CC BY, https://creativecommons.org/licenses/by/4.0/)

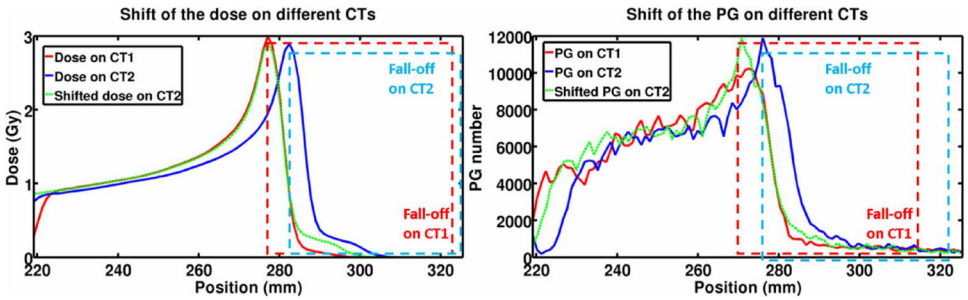

Fig. 3 MC simulations using two CT scans of the same patient taken at different times. Dose (left) and PG (right) distributions of the same pencil beam on the two CT scans are shown. Additionally, the figure depicts the search region (dashed boxes) where the sum of the squared errors between distributions is calculated to estimate the dose and PG shift between the two CT scans. Reproduced from [165] under the terms of the Creative Commons Attribution 3.0 licence (CC BY, https://creativecommons.org/licenses/by/3.0/)

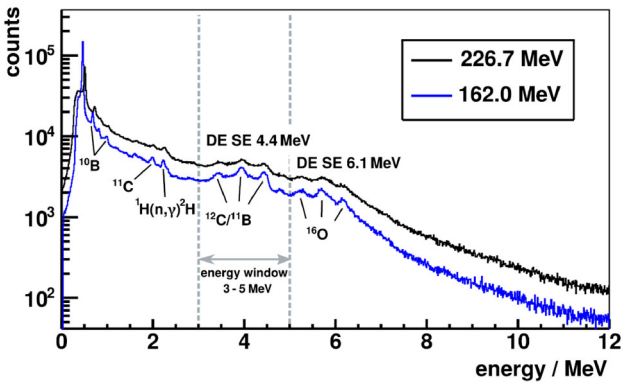

Fig. 4 Measured PG energy spectra for 226.7 MeV (black) and 162.0 MeV (blue) proton beam energies. The ground state transition in ^{16}O, ^{11}B and ^{12}C are pointed out, including their respective single (SE) and double escape peaks (DE). PG ray transitions from ^{10}B, ^{11}C and ^{1}H(n,γ)^{2}H are also visible in the low energy part. The spectra shown had no background subtraction procedure. The authors used the energy window between 3 and 5 MeV for subsequent analysis. Reproduced from [176] under the terms of the Creative Commons Attribution 3.0 licence (CC BY, https://creativecommons.org/licenses/by/3.0/)

One aspect that makes PG imaging challenging is the broad PG energy spectrum, which requires specialised detection devices. The energy spectrum can be considered up to 10 MeV for practical purposes, even though higher energies, albeit at a low yield, are also present. Contrary to PET monitoring, where the energy of the two photons emitted is well defined, PG radiation poses severe conditions on the detector design, regardless of the approach followed. A comparison of measured PG energy spectra for two proton energies is depicted in Fig. 4. The spectra were obtained at the University Proton Therapy Dresden (UPTD) using a $CeBr_3$ scintillation crystal coupled to a Hamamatsu R13089-100 photomultiplier tube. The target was a homogeneous polymethyl methacrylate (PMMA) phantom [176]. Werner *et al.* [176] mentioned that another study [138] using a similar crystal found an energy resolution of 2.21% (full width at half maximum, FWHM) at 4.44 MeV.

Another aspect that makes PG imaging demanding is the relatively low PG emission yields. Still, the PG radiation signal exhibits approximately ten times higher emission yields than the PET monitoring signal and 60–80 times if washout and acquisition time delay are considered in the calculation in the context of proton therapy [96]. However, commercial PET scanners that can be used for offline PET monitoring typically offer higher detector acceptance and efficiency than most, if not all, PG camera devices proposed thus far. Agodi *et al*. [1] reported experimental PG emission yields after irradiation of a PMMA phantom with an 80 − MeV/u carbon ion beam of $(2.32 \pm 0.01_{stat} \pm 0.15_{sys}) \times 10^{-3}$ counts ion^{-1} sr^{-1} (values provided with estimated statistical (*stat*) and systematic (*sys*) uncertainties). In turn, Pinto *et al*. [117] found experimental PG emission yields in a PMMA phantom equal to $(124 \pm 0.7_{stat} \pm 30_{sys}) \times 10^{-6}$ for 95 MeV/u carbon ions, $(79 \pm 2_{stat} \pm 23_{sys}) \times 10{-}6$ for 310 MeV/u carbon ions, and $(16 \pm 0.07_{stat} \pm 1_{sys}) \times 10^{-6}$ counts ion^{-1} mm^{-1} sr^{-1} for 160 MeV protons. When Pinto *et al*. [117] adapted their results to the conditions detailed in Agodi *et al*. [1], the results for 80 and 95 MeV/u from the two independent groups agreed remarkably well within the estimated uncertainties. Pinto *et al*. [117] went further and, based on treatment plan cases found in the literature, estimated a total of $800 \pm 4_{stat} \pm 50_{sys}$ and $8 \pm 0.2_{stat} \pm 2_{sys}$ counts mm^{-1} sr^{-1} for a spot in proton and carbon ion treatment plans, respectively. The statistical level for a spot is relevant since, ideally, PG imaging aims to monitor single spots for higher treatment quality assurance. In the case of Pinto *et al*. [117], the authors considered that a typical spot comprises 5×10^7 protons or 1×10^5 carbon ions depending on the ion employed for the treatment.

After the proposal of Jongen and Stichelbaut [53] based on MC simulations, the first experimental verification of PG imaging in particle therapy was reported in 2006 by Min *et al*. [93]. In this seminal work, Min *et al*. used a CsI(Tl) scintillator inside a massive shielding arrangement comprising paraffin, lead and boron carbide sections to scan a water phantom longitudinally with an impinging proton beam. The photons were allowed to reach the scintillator through a hole in the shielding structure; hence, the shielding structure also acted as a collimator. They observed a clear correlation between the PG distribution fall-off close to the end of the proton range and the measured depth-dose distribution for each proton energy considered (100, 150 and 200 MeV). Furthermore, they also explored the issue of neutron and neutron-related events by measuring with and without paraffin and applying minimum energy thresholds on the data postprocessing. The latter is based on the fact that most of the neutron interactions in the detector and most of the neutron-induced events, namely after neutron-gamma interactions in any material in the path of neutrons, are below a given energy. Such energy thresholds have minimal impact on the PG signal since a substantial signal is still available, thus improving the signal-to-background ratio. At this time, and only until recently, neutrons were always considered as an undesirable background because no clear correlation with the ion range was found. More on the recent paradigm shift regarding neutrons in section 4.5.

The next breakthrough in the field of PG imaging was reported two years later, in 2008. Testa *et al*. [160] irradiated a PMMA phantom with a 73 MeV/u carbon ion beam. The authors used a NaI(Tl) scintillator behind a collimator and shielding to scan the PMMA phantom longitudinally. They again showed a clear correlation between the PG distribution fall-off and the end of the ion range. This experiment employed a carbon ion energy below clinical energies, but as a feasibility experiment, it permitted the assessment of PG signals while keeping the background manageable. However, a significant novelty these authors brought was how the problem of neutron background was addressed: utilising time-of-flight (TOF) techniques to discriminate between PG and neutron-related events. Actually, without TOF techniques and only with energy thresholds as in [93], it was not possible to achieve an SBR allowing for a meaningful PG distribution, even at such low carbon ion energy.

4 PG imaging approaches

The complexity of PG imaging is a double-edged sword: it makes the research, development and deployment of any PG-based measurement device challenging, but, on the other hand, allows for a wide variety of approaches. The different approaches can be grouped into categories associated with the main focus on the PG emission analysis, ultimately leading to a metric or metrics correlated to the ion range: PG radiation spatial distribution, PG energy spectroscopy, PG timing and PG emission yields.

It is important to note that, from a technical point of view, not all approaches result in an image. Thus, the term “PG imaging” is not entirely correct for all cases discussed. Nevertheless, PG imaging, PG-based range monitoring and PG monitoring will be used interchangeably since the terms herein mainly refer to the field instead of specific monitoring solutions.

4.1 Spatial distribution of PG radiation

PG radiation is emitted after nuclear interactions, and those interactions can only occur in locations where the beam is present and almost until the end of the particle range. This phenomenon creates the opportunity to probe the beam’s location, including the end of the range, by measuring the spatial distributions of PG emission. The location of the end of the ion range is the most relevant quantity in treatment quality assurance in the context of range uncertainties. Therefore, substantial research was put into retrieving a one-dimensional (1D) PG emission profile along the beam path. This simplified approach also allows for working with distributions exhibiting higher statistical levels, which, in theory, contributes to higher confidence levels on retrieved metrics.

Min *et al*. [93] and Testa *et al*. [160] pioneer experiments aimed at having spatial distributions of PG radiation by employing mechanical collimation. In their cases, a single hole and a single slit, respectively, were used, and the phantom was scanned

longitudinally by positioning the phantom on top of a moving stage. In a clinical application of this technique, moving the patient is inconceivable. Therefore, the detector configuration should be sufficiently large to measure PG radiation, at least over the region where the PG distribution fall-off is expected, but, ideally, sufficiently large to detect the entire ion range. The reason for detecting PG radiation over the entire path boils down to the interpretation of the PG distributions measured: if only a small region around the PG distribution fall-off is available, in order to correlate this fall-off with the end of the ion range, then one needs to rely on in-room alignments and different coordinate systems, and assume that no patient setup error occurred. With the entire PG distribution, inferring the PG distribution entrance is possible, and this entrance can be correlated with the position where the ion beam enters the patient. The difference between PG distribution fall-off and entrance is an absolute measure of the length of the PG distribution, thus directly correlated with ion range without relying on other sources of information that may carry uncertainties. As an exemplary scenario, if the patient is mispositioned by 1 mm in the beam direction and only the PG monitoring data of the expected end of the ion range is available, then the PG distribution will show around 1 mm shift, even though there is no anatomical change. When the entire beam path is imaged, the PG radiation distribution will show around 1 mm shift at the end of the ion range and around 1 mm shift at the beginning of the distribution. In this scenario, the case where only the expected end of the ion range is imaged is not entirely hopeless to detect the problem: the PG monitoring data of every spot will be shifted by around 1 mm, and such a global shift may lead to infer that a patient setup error occurred. The potential advantage of PG cameras that image the entire path only pertains to the setup errors in the beam direction. In the presence of a patient setup error in the lateral direction, both approaches will likely observe changes compared to the expected distributions simply because the ion path will differ for each spot. Furthermore, the theoretical argument that only relying on the PG distributions is the ideal scenario (*i.e.* PG camera able to image the entire beam path) is disputed since the entrance can be obtained using other imaging modalities, like X-ray imaging, cone-beam CT, or optical trackers, and the plan information without the added cost, weight and footprint of a PG camera able to measure the entire range [150]. The retrievable information from the PG entrance is also less precise than the one at the distal fall-off [118], and such a fact must be considered when assessing the real advantages of using a much longer PG camera.

4.1.1 Mechanical collimation

Outside of proof-of-principle detection system arrangements employed only in experimental campaigns, the first prototype of an actual PG camera followed a design resembling a nuclear medicine pinhole camera [17]. This strategy falls into the category of PG cameras detecting PG radiation only around the PG distribution fall-off (unless two independent cameras are used, which does not bring apparent benefits compared to just relying on other imaging modalities). Even though it cannot provide information on the entrance, it brings advantages relevant to clinical implementation.

The main advantage is the footprint of such a device. It may sound less important than camera precision, resolution or efficiency, but if a PG camera is supposed to be positioned next to the patient in the treatment room, how bulky and heavy the device is matters significantly. Additionally, a smaller footprint is often associated with a more favourable ease of handling for the clinical staff, and a heavier system may pose severe constraints on the positioning ability due to weak spots on the treatment room floor or difficulty mounting it on some structures in the room. These practical factors inevitably weigh on the adoption of such devices by clinical facilities. An argument can be made that the treatment gantry, or other heavy structure in the room, can hold a hefty device for treatment monitoring purposes [15], and it can be redesigned after careful engineering calculations. However, it is unrealistic to assume that industrial partners will redesign their treatment gantry to allow early adoption of an unproven approach with an unclear clinical workflow and with an unknown client base, even if, in theory, PG imaging brings significant benefits.

The other two advantages are detection acceptance and the ability to magnify the region of interest [17]. Favourable detection acceptance is obtained with a large slit opening that completely discards any aim at improved image resolution. In this case, the concept of image resolution is to distinguish the different PG emission features linked to ion energy and tissue composition. However, this is a sensible approach for range shift detection: the goal is not to detect local, anatomical-related changes but the overall range shift of the ions being delivered. Detecting that something moves does not necessarily require pristine resolution. Due to the shape of the slit, the authors decided to call this camera a knife-edge slit camera.

Soon after, Smeets *et al*. [149] published their study on a knife-edge slit camera design and first experimental results. This PG camera differed slightly from the first one proposed by Bom *et al*. [17] using Monte Carlo simulations since it abandoned the usage of a conical-shaped collimator. This design difference allows for easier manufacturing and, arguably, for a smaller footprint. The knife-edge slit shape remained the same. The work of Smeets *et al*. [149] was massive and had significant repercussions in the field: the authors delved into almost all aspects of the usage of this camera. They described fundamental research associated with the development of the camera (for example, energy spectra measurements and neutron background assessment), postprocessing analysis regarding energy thresholds and background subtraction, a design study based on MC simulations, optimisation of collimator and detection system distances from each other and beam axis, correlation assessment of PG distribution shift and proton range shift, the correlation between range shift estimation and the number of protons, electronics development, and clinical considerations. This work was followed by several others where the knife-edge slit camera was further improved, thoroughly tested, and an entire workflow developed [80, 112, 127–129] so that clinical translation could become a reality. Figure 5 depicts a 3D drawing of the entire knife-edge slit camera setup and a photo of the knife-edge slit collimator.

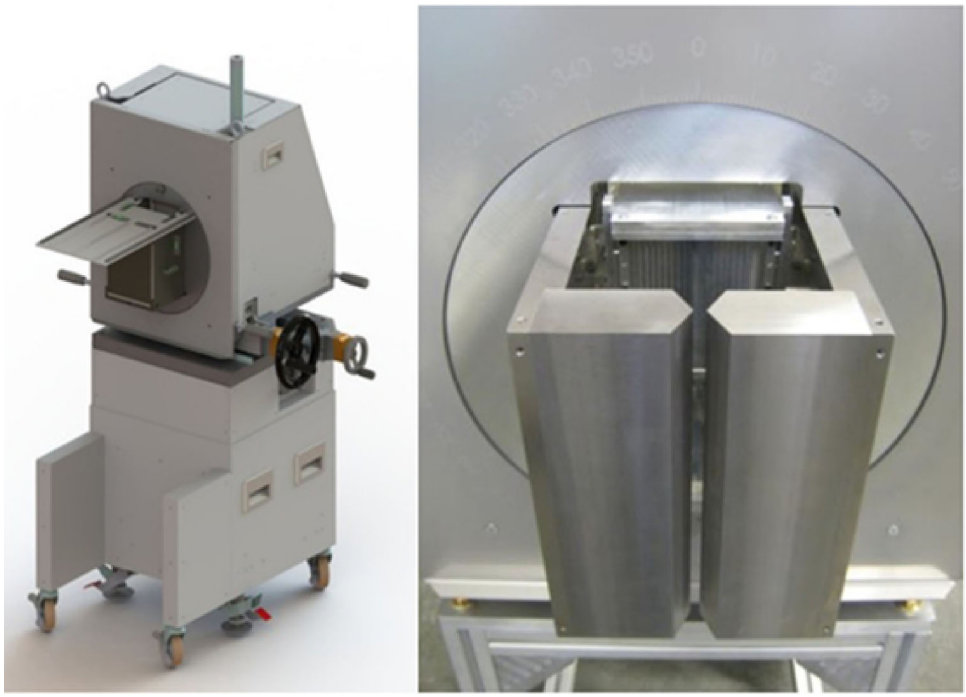

Fig. 5 Knife-edge slit camera prototype. The complete trolley positioning system is drawn on the left, and a photo of the knife-edge slit collimator is shown on the right. Reproduced from [150] under the terms of the Creative Commons Attribution License (CC BY, https://creativecommons.org/licenses/by/4.0/)

The first usage of the knife-edge slit camera in a patient was finally reported in the year of 2016 from the proton therapy centre at the Universitäts Protonen Therapie Dresden (UPTD) at OncoRay (Dresden, Germany), where a patient undergoing a passive scattered proton therapy treatment had the PG camera monitoring the treatment [134]. The treatment was a mix of photons and a proton boost for seven fractions. During those seven fractions, the patient was monitored for six while the remaining one was done with the collimator closed to assess the background. Three CTs were acquired during that period to enable an understanding of whether any anatomical change that could potentially lead to a range shift was present while monitoring.

The first clinical application of the knife-edge slit camera using a pencil beam scanning delivery was reported one year after by Xie *et al*. [178], where a patient being treated at the Roberts Proton Therapy Center, Philadelphia, Pennsylvania, USA, was monitoring for six fractions in the last three weeks of treatment (twice per week). The possibility of treatment monitoring spot by spot was clinically confirmed, and the authors stated that a shift retrieval precision of 2 mm could be achieved [178].

After these two pioneer studies, many more patients have had their proton therapy monitored through PG imaging, which has contributed to the improvement of workflows and to the development of new approaches using PG monitoring data acquired from the knife-edge slit camera [14].

Most of the research and development associated with the knife-edge slit camera was made in collaboration with the industrial partner Ion Beam Applications (IBA). To this day, this system is the only PG camera ever used to monitor a particle therapy treatment on a patient.

The knife-edge slit camera is not the only mechanically collimated system proposed for PG imaging. The teams behind the two first experimental verifications of PG imaging, Min *et al*. [93] and Testa *et al*. [160], had a different design in mind: a multi-slit collimator camera (or sometimes also called a multi-slab collimator camera). In this design, an array of slabs of material are placed together to form a collimator with multiple openings (slits) in a row. The openings are oriented perpendicularly to the beam axis, allowing the passage of photons while keeping the correlation with the position from where they were emitted. This arrangement creates a one-dimensional detected PG distribution in which each opening, and thus each detector segment, can be correlated with a well-defined location along the ion beam path inside the patient [118]. Figure 6 depicts a schematic representation of a dual-head multi-slit collimator camera which was used for an MC-based study for the development of a machine learning algorithm to create optimized treatment-specific classifiers that detect discrepancies between planned and delivered dose [35]. An interesting aspect of this figure is the existence of a beam tagging device for PG imaging, envisioning the use of TOF techniques. It should also be noted that the multi-slit collimator camera depicted does not allow for the detection of the PG signal at the entrance, which would necessarily either be extended farther or shifted towards the nozzle.

Between the knife-edge slit camera and the multi-slit collimator camera, it is difficult to answer which PG camera approach is better. Huisman *et al*. reported that, when using an optimized multi-slit collimator camera, this device will outperform a knife-edge slit camera in realistic conditions [46]. In turn, in a different study where a multi-slit collimator camera was designed following

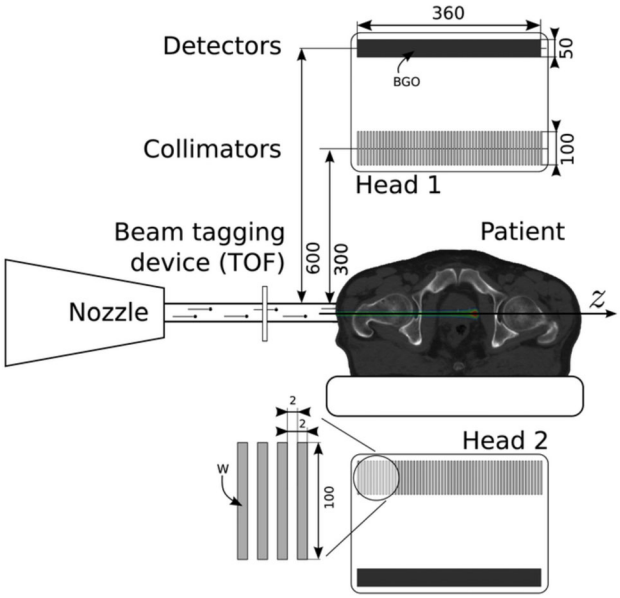

Fig. 6 Schematic representation of the simulation setup using a dual-head multi-slit collimator PG camera. Protons coming from the nozzle trigger the beam-tagging device for TOF applications. PG radiation is collimated by the tungsten slabs (in light grey), while the BGO scintillator crystals (dark grey) detect the photons in an Anger-like fashion. Adapted from [35] under the terms of the Creative Commons Attribution 3.0 License (https://creativecommons.org/licenses/by/3.0/)

the constraints imposed by an optimized design of a knife-edge slit camera (for example, enforcing the same attenuation efficiency of the collimator for both camera designs), the knife-edge slit camera performed better or equally well as the multi-slit collimator camera [150]. The second study mentioned may seem unfair because the comparison is between an optimized knife-edge slit camera and a subpar design of the multi-slit collimator camera. However, the purpose of the authors of the second study was to compare the two PG camera designs in *"conditions of equal performance"* [150]. Regardless of the conclusions derived from MC-based studies, the final answer will come when multi-slit collimator cameras are deployed in a clinical setting and data from patient PG monitoring are available for analysis and comparison to knife-edge slit camera data.

Min *et al*. [94] reported an optimization study on a multi-slit collimator camera using CsI(Tl) scintillators and experimental results on a simplified setup. Pinto *et al*. [118] presented an MC-based optimization study based on experimental data, while Krimmer *et al*. [63] used a simplified setup of a multi-slit collimator to test multi-detector configurations experimentally. More recently, Ku *et al*. [66] reported an improved design for a multi-slit collimator camera over the previous prototype of Park *et al*. [106]. The new design overcomes the limitations of its predecessor by enhancing PG detection sensitivity and incorporating a precise camera positioning system [106]. Ku *et al*. [66] also developed algorithms able to estimate ion ranges based on PG radiation detection with their device, and this system offers good prospects of becoming the first multi-slit collimator PG camera to be used with patients. Malekzadeh *et al*. [87] presented an intriguing proposal where a PG camera could be built using a combination of multi-slit and knife-edge slit collimators. Finally, recently Sun *et al*. [155] proposed a two-dimensional (2D) PG camera that allows for the acquisition of 2D PG images. The authors reported exciting results in this MC-based study, showing that the system performs well for proof-of-principle conditions (idealized beam, simulated background). High-quality 2D PG distributions are shown, along with the data analysis used to retrieve range shifts. More data is needed to assert how well this approach will succeed, but it demonstrates interest in innovative solutions for PG imaging.

4.1.2 Electronic collimation

The systems with electronic collimation use the Compton scattering process and are termed Compton cameras. They comprise a scatterer and an absorber detector in the most straightforward design possible. Ideally, the incident photon scatters in the scatterer and is then fully absorbed in the absorber. The scatterer absorbs the recoil electron, and its energy is measured. With the knowledge about recoil electron and photon energies, the scattering angle can be derived based on Compton scattering kinematics, and a cone is formed with all possible positions from where the photon has originated. The direction of the photon after being scattered (between the scatterer and the absorber) defines the cone's axis. Figure 7 shows a schematic representation of this process. The accumulation of events makes each cone intersect, and reconstruction methods are employed to build the image. From all approaches in PG imaging, Compton cameras are the only system that allows for 3D imaging with a single device. In a rough approximation, this reconstruction process is similar to the one used for PET imaging, but instead of a line-of-response, there is a cone-of-response. However, the cone will be wrongly estimated if the photon or the recoil electron is not fully absorbed, and no cone will be derived if there is

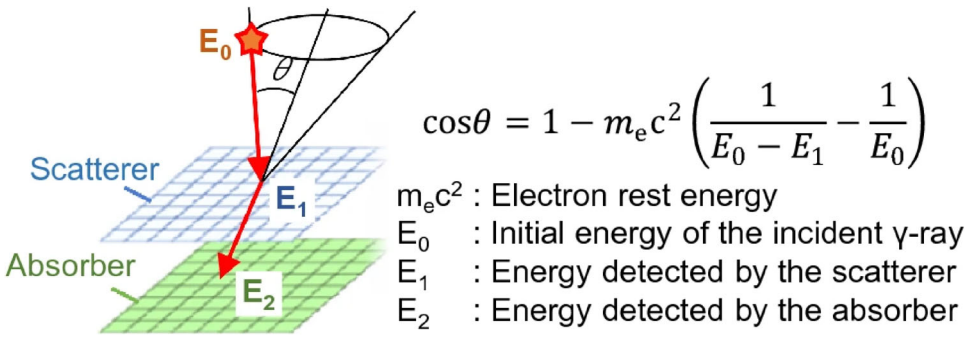

Fig. 7 Principle of operation of a two-stage Compton camera. Reproduced from [141] under a Creative Commons Attribution 4.0 International License (https://creativecommons.org/licenses/by/4.0/)

no scattering in the first detector. To overcome this problem, some authors have proposed solutions where the photon undergoes multiple scattering interactions or, at least, the multiple scatterers are used to increase the probability of a Compton interaction [91, 114, 132, 133, 136]. If the photon scatters twice or more, then it is possible to circumvent the need for complete absorption in the absorber detector [114].

Several approaches have been proposed concerning the Compton camera design. Roellinghoff *et al*. [136] published a study analysing the potentialities of a single-scattering Compton camera using multiple scatterers, while Richard *et al*. [133] proposed two silicon detectors to act as scatterers in order to increase the camera efficiency by allowing double scattering (both studies considered an absorber made of a scintillator crystal). Kurosawa *et al*. [67] presented the very first experimental PG distribution after proton irradiation in a water phantom with a Compton camera. Their Compton camera distinguishes itself from other Compton camera proposals by employing a gas chamber where the Compton scattering occurs [67]. Peterson *et al*. [114] optimised a 3-stage Compton camera (two scatterers and one absorber), which was later used in a clinical beam. The report on clinical beam irradiation was done by Polf *et al*. [123], where the authors irradiated a water phantom with two clinical energies at clinical dose rates. A follow-up experiment reported by Draeger *et al*. [26] demonstrated the feasibility of 3D PG imaging with a Compton camera using clinical beam conditions. Kormoll *et al*. [58] studied the performance of several Compton camera solutions for proton therapy monitoring. They found that a design comprising cadmium zinc telluride (CdZnTe) layers as scatterers and an LSO scintillator as an absorber could be a good candidate [58]. Llosá *et al*. [76] have developed a Compton camera prototype using only scintillator crystals ($LaBr_3$ and LYSO) for both scatterer and absorber with promising results for point-like sources [76]. The design was later improved and the updated prototype features three layers, all made of $LaBr_3$ scintillator crystals, and promising results, including with test beams, have been reported [11, 12, 77]. Thirolf *et al*. [163] have developed a Compton camera that also tracks the recoil electrons to increase the camera efficiency. The SiFi-CC project is researching and developing a Compton camera where both the scatterer and absorber are comprised of a stack of scintillation fibres [55].

From a conceptual point of view, the Compton camera would be the perfect PG camera. Its electronic collimation makes the detector acceptance substantially better than for cameras relying on mechanical collimation. In theory, the absence of mechanical collimation could permit a small footprint device, which would be favoured for a clinical setting. Its inherent capability of yielding 3D images would bypass the need for multiple devices. Unfortunately, the reality is considerably more challenging. The absence of any form of mechanical collimation also implies that the counting rate of both signal and background is exceptionally high, which is taxing on the whole chain of the detection system [31, 91, 105]. The probability that scattering occurs is relatively low, notwithstanding that it can be improved with different design choices [133]. Furthermore, the broad PG energy spectrum makes the Compton camera design optimisation a daunting process: even if the absorber can be made sufficiently large to stop a majority of the PG radiation, the design of a scattering system that, for example, works as well for 1-MeV photons as it works for 8-MeV photons is hardly possible [3]. The application of Compton cameras for medical applications was first proposed in 1974 by Todd *et al*. [167], and it is still in the development phase. Considering that said proposal was for nuclear medicine applications, which may be seen as a more favourable radiation environment than proton therapy monitoring, it is no surprise that Compton cameras for PG imaging pose formidable challenges (Fig. 8).

4.2 PG energy spectroscopy

Exploiting the energy information of the emitted PG is a growing interest due to the possibility of retrieving both ion range and tissue composition. The rationale of this approach is built upon the characteristic emission from known nuclear transition levels, which leads to the emission of photons with well-defined energy [170]. Since the transitions are associated with a given target nucleus, its concentration will impact the yield of PG emitted. Polf *et al*. [121, 122] demonstrated that the 6.13 MeV PG emission line from the proton on ^{16}O nucleus reaction is proportional to the concentration of oxygen in tissue irradiated with proton beams, showing that it is possible to determine the concentration of oxygen in tissues irradiated with proton beams by measuring this emission. A more

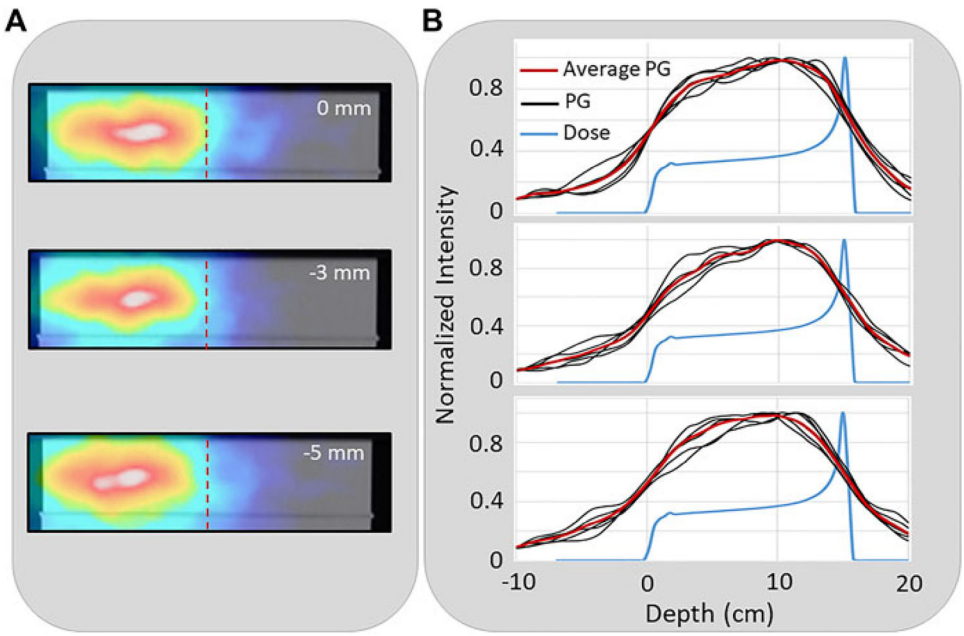

Fig. 8 **A** An example of a 2D reconstruction of PG emission measured during the delivery of a 150 MeV proton beam (0 cm) and with the range shifted by $-3\,mm$ and $-5\,mm$. The dashed vertical line indicates the depth of distal 80% of the proton depth-dose profile in the target. **B** 1D profiles extracted from five independent PG images for the full range (top), 3 mm (middle) and 5 mm (bottom) range shifted beams. Reproduced from [124] under the terms of the Creative Commons Attribution License (CC BY, https://creativecommons.org/licenses/by/4.0/)

comprehensive study has been published by Magalhaes Martins *et al*. [84], where the authors looked into elemental concentration determination made possible by PG spectroscopy not only in proton beams but also in helium and carbon ion beams. Specifically, the authors derived oxygen, carbon, and calcium concentrations. They were able to identify elemental concentration changes of 1% for calcium and 2% for oxygen in adipose, brain, breast, liver, muscle and bone-related tissue surrogates [84]. In a parallel study, Magalhaes Martins *et al*. [85] proposed the usage of endorectal balloons filled with a silicon solution for the monitoring of prostate radiotherapy treatments. When protons interact with the silicon atoms inside the endorectal balloon in a proton range shift scenario, they emit PG radiation with a characteristic energy of 1.78 MeV. By using detectors searching for this energy signal, the authors have shown the feasibility of employing this approach for single-spot monitoring as well as whole-treatment delivery [85].

Verburg and colleagues [169, 171] extended the usage of PG energy information to absolute ion range measurements. They are developing a concept in which the PG emission yields of several characteristic lines correlate with the proton range. By parameterising the expected ratios between different PG characteristic line yields, they created a method that can unequivocally provide the information at which depth the field-of-view of their detector measures along the beam path [169]. To improve the SBR of their distributions, they use TOF techniques to make the PG selection. The workflow in place can also retrieve carbon and oxygen concentrations [159], and a full-scale prototype is ready to be deployed in a clinical scenario [44]. The research team behind this PG camera has demonstrated that it applies to both passive [162] and active delivery irradiation [44, 159].

4.3 Exploring PG time features

The deeper the protons travel inside a patient's body, the wider the time distribution of the PG signal will be. Furthermore, the end of the time distribution of the PG signal is linked to how far the protons travelled, the so-called transit time. This idea of varying time distributions depending on ion transit time is the rationale of the approach coined as PG timing, which was first proposed by Golnik *et al*. [34]. This ingenious idea is as simple as it is elegant: a single, small detector may be able to provide meaningful information regarding ion range shifts. Figure 9 depicts the concept behind this approach and some exemplary PG timing distributions.

In a best-case scenario calculation, the authors estimated the ability to detect proton range shifts of 3 mm with the current experimental setup. This setup can be further optimised to become a clinical prototype, and improvements may lead to precisions on range shift assessment of 1–2 mm [43]. This approach is under active development [43, 176], and it may become one of the most cost-effective and with the smallest footprint of all solutions for PG radiation-based monitoring.

Another exciting approach exploring the features of PG time distributions has been proposed by Jacquet *et al*. [49]. Therein, the authors have reported the usage of a beam-tagging device for TOF trigger and a technique which reconstructs the PG vertex position by employing many detectors placed at different positions. While PG timing detects range shifts by calibration methods [34], the solution put forward by Jacquet *et al*. [49] tries and reconstructs the PG vertex position directly. Further research has been conducted,

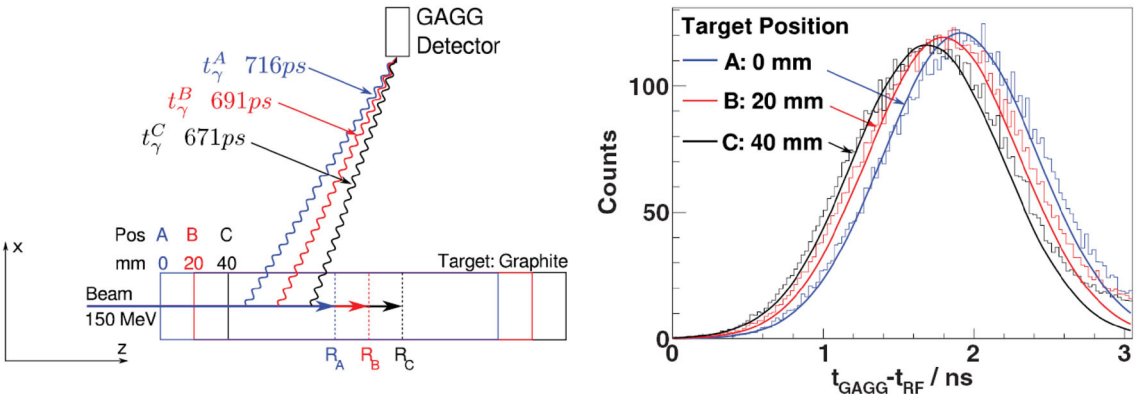

Fig. 9 (Left) Setup of the irradiation experiment with a graphite phantom using a 150-MeV proton beam. The phantom was irradiated at three positions: A, B, and C. TOF examples of PG radiation at different positions are indicated. (Right) Experimental PG timing spectra for phantom positions A, B, and C are depicted as histograms. Reproduced from [34] under the terms of the Creative Commons Attribution 3.0 licence (CC BY, https://creativecommons.org/licenses/by/3.0/)

and a modified version of this solution was published [111]. In Jacquet *et al*. [49], an MC simulation of the beam-target interactions is used to process the detection time and reconstruct the emission point of each detected PG. This MC simulation assumes knowledge of the target and that range shifts are still, albeit indirectly, quantified through a calibration curve [49]. Therefore, Pennazio *et al*. [111] propose to employ a maximum-likelihood expectation maximisation (MLEM) algorithm to bypass any knowledge regarding the patient tissues in the reconstruction of PG vertex positions. Pennazio *et al*. named this form of reconstruction spatiotemporal emission reconstruction [111].

4.4 Yields of PG radiation

The approach of PG timing aims to analyse the PG timing distributions based on position and width, essentially, the mean and sigma of the PG timing distributions. A more straightforward method may be just integrating the amount of PG signal inside the TOF region associated with the PG radiation (hereafter in this subsection referred to as PG TOF region). Krimmer *et al*. [64] proposed such a solution, where they demonstrated that obtaining the PG radiation yield by integrating the PG signal in the time domain leads to a detection system capable of identifying proton range shifts of 3 mm in a PMMA phantom. Krimmer *et al*. [64] tested this approach using a proton passive delivery system where a modulator wheel changes the range of protons in a PMMA target. For the different positions of the modulator wheel, the authors observed that the PG count rate inside the PG TOF region was different and correlated with range. The authors attributed the change in PG count rate to two reasons: (1) the difference in the proton range inside the target, hence a difference in the total number of PG emitted and (2) the loss of protons via scattering in the modulator wheel depending on the amount of material traversed in the wheel. The authors called this approach prompt gamma peak integration (PGPI) [64].

This method has been extended by introducing a beam-tagging device, in this case, a diamond detector, which results in a significant improvement of the TOF analysis, thus enhancing the stability and sensitivity of this form of monitoring [88].

4.5 Multimodality and neutron imaging

The usage of multimodality in particle therapy monitoring has often been mentioned and discussed, but the challenges of dealing with one approach alone have delayed comprehensive studies on this topic. However, recent concrete examples of the exploitation of ion range assessment by combining PET and PG imaging have been reported. The work of Ferrero *et al*. [30], followed by the work of Pennazio *et al*. [111] described in section 4.3, uses a PET scanner aimed at PET monitoring and adds the spatiotemporal emission reconstruction for PG imaging. Figure 10 shows the simulation setup in Pennazio *et al*. [111], including the arrangement of the PET detectors that are also used for PG imaging.

In turn, Choi *et al*. [21] published an MC-based study aiming at the integration of PG and PET monitoring and how to accomplish it. They proposed that simply creating a ring of PG cameras and using a PET detection module could achieve this goal. In addition, they made an extensive simulation study on the usage of background reduction techniques in such a PG-PET system, namely energy window, depth-of-interaction (DOI), and TOF.

Neutrons were always seen as contributing to an undesirable background. Min *et al*. [93] created an extensive collimation system where paraffin was also included to moderate neutrons. Testa *et al*. [161] also included setups with paraffin in carbon ion irradiation experiments to reduce the neutron-related background. However, contrary to Min *et al*. [93], Testa *et al*. [161] also tried to assess if ion range-related information could be obtained from neutrons. The authors used a liquid organic neutron scintillator,

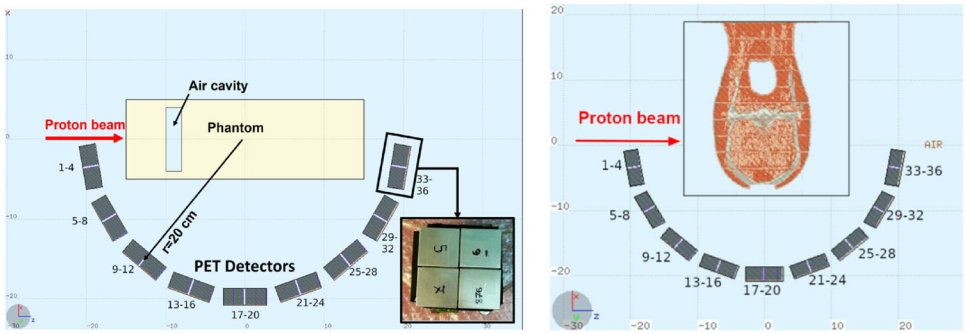

Fig. 10 Schematics of the simulated setup. The proton beam is impinging towards the positive Z direction in a homogeneous PMMA phantom in which an air cavity of variable thickness can be present (**a**), and in an anthropomorphic phantom with soft tissues, bone, and brain-like materials (**b**). In both cases, the phantom is surrounded by a half-circle of PET modules. In the inset in (**a**), the front view of a PET module is shown. Reproduced from [111] under the terms of the Creative Commons Attribution License (CC BY, https://creativecommons.org/licenses/by/4.0/)

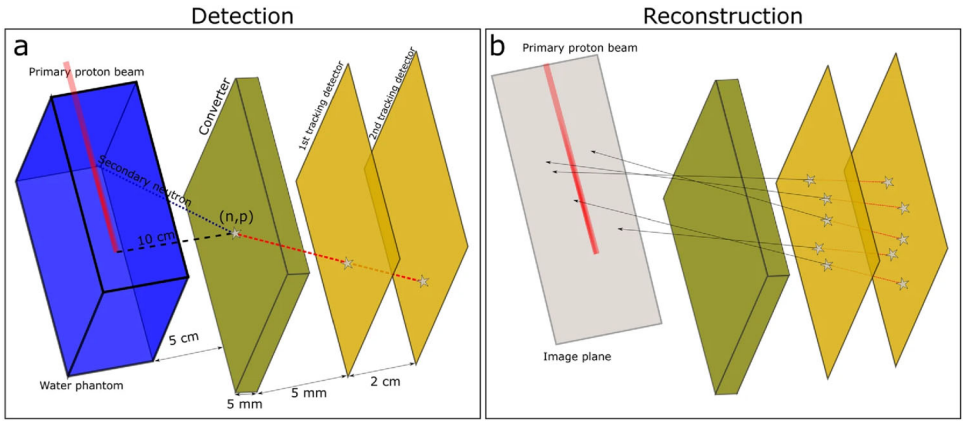

Fig. 11 **a** The conceptual design of the NOVO approach. Neutrons produced along the beam path in the water phantom may be converted to protons in the converter material. **b** Protons reaching both tracking detectors give positional information used for reconstruction. Reproduced from [182] under the terms of a Creative Commons Attribution 4.0 International License (CC BY, https://creativecommons.org/licenses/by/4.0/)

a BC501 detector, to extract any information from neutrons. After careful data analysis, the authors stated that "no evidence for a prompt neutron component correlated with the primary ion range was found for the GANIL experiment, where a dedicated paraffin collimation was used. Therefore, fast neutrons detected at 90°cannot be considered to provide useful information on the dose profile. However, this does not imply that neutrons could not provide some information at a more forwarded angle, but this remains to be investigated in another study" [161]. This research from 2010 shows that the neutron signal was subject to experimental campaigns, even though those early investigations did not yield conclusive results. After Testa *et al*. [161], research groups working on PG imaging continued to develop methods to reduce neutron background, from assumptions of constant background (for example, [149]) to energy thresholds and TOF. This reality changed recently when the NOVO collaboration was created and published their first results [182]. Their method is based on converting the neutrons to protons in a converter layer and then tracking the protons using at least two tracking detectors. The interaction points of the proton in the tracking detectors create a line that projects into the target to get a reconstructed profile. Figure 11 depicts this neutron-detection logic.

An intriguing aspect of this approach can be deduced from Fig. 11: the goal is not necessarily to reconstruct an accurate neutron distribution in the target but to have a profile correlated with the ion range. The authors use the concept of a range landmark, which is the sum of the sample mean for the ensemble of reconstructed coordinates and their corresponding standard deviation [182]. Figure 12 shows the neutron, reconstructed and depth-dose distributions of three different energies and the landmark positions for each case.

The reason for bringing the topic of neutron imaging into a manuscript reviewing PG imaging is that neutron imaging alone has shortcomings for a feasible ion range monitoring device due to limited counting statistics for a typical clinical proton pencil beam [70, 92]. Lerendegui-Marco *et al*. [70] proposed a system inspired by a detector for industrial and nuclear security applications where PG, and thermal and epithermal neutrons are detected in parallel. Soon after, the NOVO collaboration reported a similar approach [92] in which the authors improved on the initial proposal of fast neutron detection only to now also include PG imaging in the same detection system. In an MC-based study, the authors showed that the combination of neutron and PG imaging in their system is

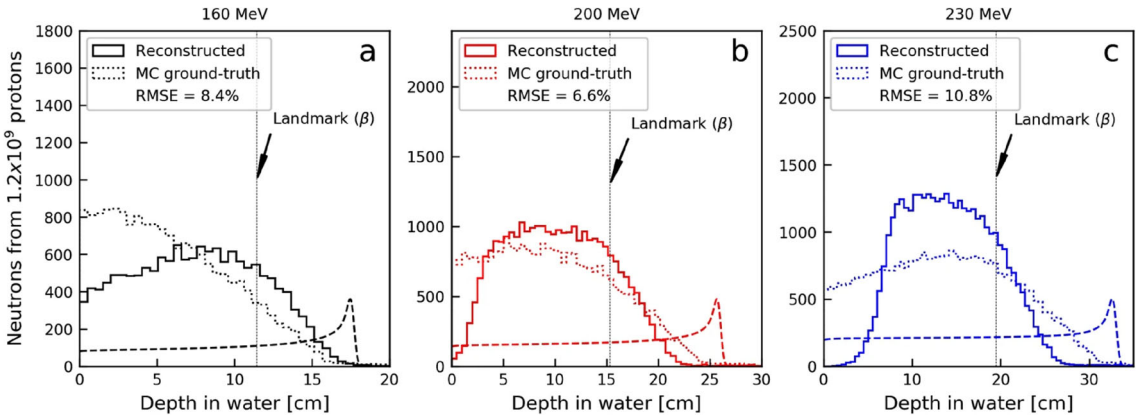

Fig. 12 The distributions of production depths for detected neutrons produced in 160 (**a**), 200 (**b**) and 230 (**c**) MeV proton beams are shown. The neutron distributions obtained from MC simulations (dotted lines) and the reconstructed profiles (solid lines) are shown. All figures with vertical dashed lines indicate the landmark for range verification. Reproduced from [182] under the terms of a Creative Commons Attribution 4.0 International License (CC BY, https://creativecommons.org/licenses/by/4.0/)

expected to provide a sufficiently high sensitivity to fast neutrons and PG radiation and a much smaller footprint than the other state-of-the-art proton monitoring systems [92].

5 The hard reality of PG emission yields

Avoiding the proverbial elephant in the room when discussing PG imaging is difficult: low PG counting statistics aggravated by a not-insignificant background. In section 3, the work of Pinto et al. was mentioned, where they estimated 800 PG emitted per millimetre and steradian for a representative pencil beam in a proton therapy treatment. For a 5-cm radius cylindrical detector positioned 50 cm from the beam axis and assuming perfect efficiency, this implies less than 25 PG counts detected for each millimetre. No matter how good the analysis workflow is, this level of statistics poses considerable challenges. However, arguably, the most critical challenge for PG imaging is not these yields per se but what sometimes seems to be a lack of a profound understanding that this challenge exists when translating PG imaging techniques into clinical practice. Feasibility or proof-of-concept studies are, by definition, studies where idealised scenarios are explored so that correlations, trends, metrics or other quantities can be found. This type of study often defines if a scientific path is worthwhile to pursue and, if so, to guide future developments. Therefore, MC or experimental high-statistics scenarios are the most reasonable to consider at that stage. The same applies to studies aiming at yield or cross-section analysis: the data should be of the highest quality possible and, thus, invariably associated with lower variance levels. In this context, it is not uncommon to see the reported number of protons exceeding 10^{10} protons impinging on a target. For example, Smeets *et al.* [149] state that 7.30×10^{10} and 1.70×10^{10} protons were delivered at 100 and 160 MeV, respectively.

When studies aiming at clinical implementation or with obvious clinical connection (for example, usage of patient CT data in a simulation study) are reported, a clinically realistic statistical level is desired. By keeping the studies realistic, the community can better assess what is and, more importantly, what is not possible with PG imaging. As a rule of thumb, a large-weight spot in a typical proton therapy treatment should have around 10^8 protons, and only a few spots are around those values (for example, [149]). It is safer and wiser to estimate PG imaging performances considering the interval of 10^7–10^8 protons per spot, but also knowing that some spots will have less than that. A recommendation on the best approach is to follow what, for example, Smeets *et al.* [149] or Roellinghoff *et al.* [137] reported, which is a PG shift detection precision as a function of the number of protons. In the case of Smeets *et al.* [149], they reported simulated and experimental precisions from around 10^7 protons up to around 10^{10}. This type of plot indicates the limits of the technique and what is possible to achieve realistically. Claims have been made that particle therapy monitoring, not only specific to PG imaging, could achieve submillimetre precision. With the current experience and data acquired in clinical conditions, this claim is difficult to sustain in an actual clinical device when PG imaging is performed for each pencil beam or even when monitoring is considered only on the pencil beams with higher weights in a typical plan. Excluding that some approaches may achieve such a performance is impossible, namely if PG cameras with increased detection acceptance and efficiency are developed or if novel techniques are utilised in the data processing. However, is submillimetre precision a necessity when using PG imaging? The range of one to three millimetres of precision already offers a remarkable performance, which can assist in, for example, reducing safety margins, hence providing the means to explore reductions in treatment toxicity [15]. Even a worst-case scenario of a 5 mm precision in PG imaging (or particle therapy monitoring in general) would help reduce the 8 mm safety margin mentioned in section 2 and allow for the research of novel irradiation strategies that require higher treatment QA, such as hypofractionation schemes.

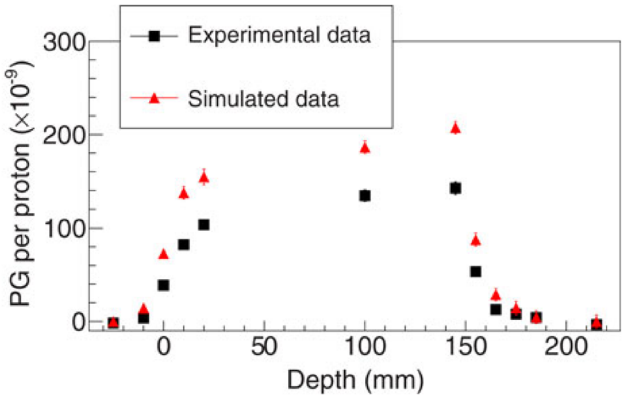

Fig. 13 Experimental and simulated PG data. The simulated data were obtained with Geant4 using the BIC model for proton inelastic interactions. Reproduced from [119] under the terms of the Creative Commons Attribution License (CC BY, https://creativecommons.org/licenses/by/4.0/)

In parallel to the problem of low yields and high background, general-purpose MC tools are notoriously recognised to fail when dealing with PG imaging. Unfortunately, failing in this context means going towards a trend of more favourable conditions than in reality: estimating higher PG yields and lower background, thus a considerably better SBR in simulations. Furthermore, one must distinguish the simulation of characteristic emission lines alone and the simulation of the entire PG emission, thus, characteristic emission plus continuum. The latter is more broadly relevant since most techniques use an energy range considering characteristic emission and continuum. For example, the knife-edge slit camera being used today integrates all events recorded within 3–6 MeV [149].

There are three main general-purpose MC tools used in the field: Geant4 [2] (and the tools built on top of Geant4, like GATE [50], GAMOS [6] or TOPAS [113]), FLUKA [29] and MCNP [135]. By far, Geant4 and its derivatives are the most benchmarked MC packages. Dedes *et al*. [24] reported that "Geant4 simulations consistently overestimate the prompt-gamma yields by a factor of about 1.8–2.8, over an energy range from 80 to 310 MeV/u for the case of ^{12}C. For the case of 160 MeV protons, the integral of the open/closed wall difference prompt-gamma energy spectrum from 1 to 10 MeV is overestimated by a factor of 1.7". Pinto *et al*. [119] found that, for proton irradiation, "Geant4 overestimates the prompt-gamma emission yields by 40.2±0.3%, even though it predicts the prompt-gamma profile length of the experimental profile accurately". A figure from Pinto *et al*. [119] illustrating the problem of different yields between simulations and experimental data is shown in Fig. 13. Perali *et al*. [112] found for 100, 160 and 230 MeV proton beams using MCNPX that the "best match between measurements and simulations was obtained by scaling the simulation for a factor 0.91, 0.76 and 0.74". In turn, Verburg *et al*. [170] stated that "estimates of the total gamma emission during proton irradiation of soft tissue and lung tissue, differed by a factor of about 2 near the end-of-range of the protons. At higher incident proton energies, the models agreed within ∼25%". When considering characteristic emission, in the same study of Verburg *et al*. [170], the authors continue: "If specific discrete gamma lines are considered, the models variations can be larger". It should be noted that the considerations of Verburg *et al*. [170] are for Geant4 and MCNP6. Schumann *et al*. [145] reported that when compared to experimental data, "Geant4 strongly overestimates the photon yield in most cases, sometimes up to 50%". More recently and focused on characteristic emission, Kelleter *et al*. [56] found that "obtained data are in reasonable agreement with the cross section data from other experiments. Discrepancies were observed when comparing our experimental data to TALYS gamma production cross sections, in particular an overshooting of the ^{16}O(p; $X_{\gamma_{4.44MeV}}$)^{12}C contribution to the 4.44 MeV line close to its threshold and an underestimation of all cross sections for higher proton energies". A follow-up study reported in Wrońska *et al*. [177] disclosed worrisome findings with the usage of different physics lists in Geant4 and newer Geant4 versions: "The comparison of simulated and measured spectra shows that the QGSP_BIC_AllHP physics list does not reproduce the features of the experimental spectra even qualitatively: the simulated spectra show an unrealistic shape evolution of the discrete lines along the proton path" and "Modifications to prompt-gamma emission modelling in higher versions of the software increase the discrepancy between the simulation results and the experimental data".

It should be stressed that modelling the continuum component in the PG energy spectrum is tricky. The continuum contains both PG signal and background events when conducting experimental work. Techniques can be employed to minimise the background, like TOF, but the background is still part of it [56]. This reality makes the benchmarking and follow-up improvements of any model very challenging.

Regarding background, Smeets *et al*. [149] observed much lower MCNPX-simulated backgrounds when compared to measured data. They employed an offset method to compensate for the missing background. As a rough estimation by looking at figure 28 in Smeets *et al*. [149], the authors used a ∼200% offset for measurements using 100 MeV protons and a ∼230% offset for 160 MeV protons (offset estimated using the simulations baseline). Pinto *et al*. [118] applied an offset of ∼30% to TOF spectra obtained with Geant4 (using physics list QGSP_BIC_HP) to bring the simulation baseline into agreement with the baseline in experimental TOF spectra. Studies regarding neutron radiation fields present in the treatment room using extended-range Bonner sphere spectrometry

systems show that iron-rich components in the room, such as the gantry cylinders, the gantry cone and the counterweight, contribute to secondary neutron contamination [28, 89]. Including room models in the PG-imaging simulations is not a standard procedure, which adds to the uncertainty of the background quantification.

When the community does not factor in the MC tool's inaccuracies when designing their PG imaging systems or when performing feasibility studies, it creates a false sense of achievement that is doomed to collide with a wall when experimental data starts to be analysed. Improving system designs and approaches due to the lessons learned from experimental data is always good. However, there is something to be gained if expectations are met with reality to some degree.

An example of improving approaches due to the lessons learned from experimental data is given in Xie *et al*. [178]. As mentioned in section 4.1.1, Xie *et al*. were the first to use PG imaging to monitor a proton therapy using a pencil beam scanning delivery. Up to that moment, PG imaging using the knife-edge slit camera on a spot-by-spot basis in a typical treatment plan was deemed possible. However, the authors realised that the counting statistics were too low for a meaningful monitoring outcome. Therefore, they used the method of spot aggregation, which had been previously suggested by Priegnitz *et al*. [127]. The study of Priegnitz *et al*. was part of the research collaborations around the knife-edge slit camera, which made employing such a method in clinical data in Xie *et al*. seamless. Spot aggregation artificially increases the spot statistics by including the PG radiation events from neighbouring spots. Xie *et al*. [178] used a Gaussian-weighted aggregation to give higher weights to the spots closer in the aggregation procedure. This procedure reduces the Poisson noise for each PG profile at the cost of degradation in lateral spatial resolution [178] and consequent loss of lateral information. However, Xie *et al*. estimated that such an approach has a limited impact on the lateral spatial resolution while improving the SBR [178], thus making it an acceptable trade-off for range monitoring when considering the knife-edge slit camera. It is still unclear if spot aggregation has a detrimental and significant impact on other forms of PG imaging. By the nature of its design, the knife-edge slit camera typically has lower spatial resolution when compared to other PG camera proposals, which can limit the impact of even lower spatial resolution (this PG camera is designed to maximise detection acceptance and efficiency and forego spatial resolution considerations). Furthermore, Gueth *et al*. [35] found that, when using a machine learning-based classifier to detect discrepancies in PG profiles, including range shifts, the classifier worked best when the information available was not only focused on the PG distribution fall-off and that information along the beam path can be crucial to find overall discrepancies [35]. The quality of such information is linked to the PG imaging spatial resolution, which makes spot aggregation a technique that deserves careful analysis when applied elsewhere.

Tian *et al*. [164–166] proposed a different method to deal with low PG yields: deliver more protons for a few selected spots. The idea is quite simple, but this proposal's pivotal aspect is selecting the spots to boost while ensuring that the treatment plan is dosimetrically equivalent to the plan without boosting. Tian *et al*. developed a so-called PG-dose correlation, which aims to correlate shifts in the depth-dose distribution to shifts in the PG distribution so that the PG signal could better indicate the presence of an ion range shift. Better PG-dose correlation is favoured in this proposal, which then drives the spot selection procedure. Other considerations are also made in the spot selection process, such as distance to air cavities, avoiding overlapping of selected spots to minimise hot spots in the plan, smooth spot surface (to avoid boosting a spot distorted by significant tissue inhomogeneity), number of selected spots, among others [164–166]. The authors demonstrated in clinical data that such a boosting procedure is feasible while keeping the dose and linear energy transfer (LET) distributions dosimetrically equivalent to the original plan. Figure 14 depicts some of the steps in selecting spots to boost. This solution envisages a future where PG-driven treatment planning can become a reality, and that is being further explored in the project funded by the Deutsche Forschungsgemeinschaft (DFG, project number 441208898), which aims at incorporating PG range verification and biological effectiveness in terms of LET and RBE as new criteria in a research proton planning system based on multicriteria optimisation (MCO).

Another approach to tackle low yields and high background levels is to use advanced selection (good PG events) and discrimination (remove background) procedures. This approach does not improve the physics limitations of PG imaging but allows for higher-quality data, which can be used to assess treatment QA. The research is focused on machine learning and artificial intelligence methods. Gueth *et al*. [35] proposed an approach to detect possible discrepancies between planned and delivered doses based on a machine learning classifier by using the PG distribution distal fall-off. Polf *et al*. [124] described a neural network that can identify bad events arising from background noise during the measurement and correctly order the different PG interactions in the Compton camera to help improve the fidelity of the data used for image reconstruction. A follow-up improved version of this approach was reported in Clark *et al*. [22], where a different neural network architecture was used with significant impacts on the time needed to run the model. Kozani and Magiera [60] published a study where they used several machine-learning approaches applied to Compton camera data and where the algorithms were trained to recognise valid Compton events.

6 PG imaging prediction

6.1 Monte Carlo engines

MC engines have been ubiquitous in the particle therapy monitoring field. However, full-blown MC tools are computationally demanding and require calculation times that extend for several days if a single computer is used and PG emission is sought [120]. An argument can be made that any clinical facility employing MC tools for patient QA will have a computational infrastructure, such

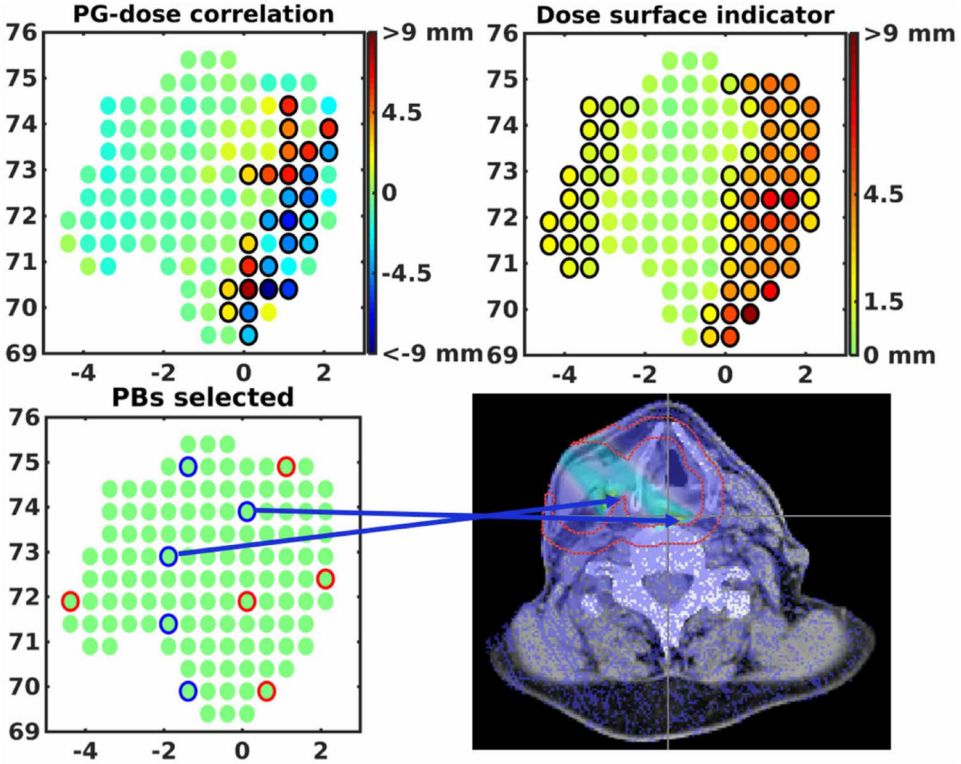

Fig. 14 The PG-dose correlation and dose surface indicators are shown in this figure. The top left plot shows the beam's eye view (BEV) of the spot-by-spot PG-dose correlation for a head and neck patient. The BEV of the dose surface indicator is shown on the top right. The pencil beams without black rings are identified as suitable spots to boost. The bottom left shows a selection of pencil beams to boost after fulfilling the different boosting criteria (blue circles) and a selection of pencil beams that fail the boosting criteria (red circles). The rationale for selecting recommended and not recommended pencil beams is for plan comparison. The bottom right shows the MC dose distribution of two selected pencil beams indicated by blue arrows. Reproduced from [165] under the terms of the Creative Commons Attribution 3.0 licence (CC BY, https://creativecommons.org/licenses/by/3.0/)

as computing clusters, to speed up calculations. Nevertheless, that would limit the adoption of MC tools to the clinical institutions able to afford such an infrastructure and personnel to run it and, by extension, increase the disparity among clinical institutions of what is available to offer to the patients. Furthermore, general-purpose MC tools typically have a steep learning curve, often requiring specialised staff to prepare, run and analyse the simulation results.

The user-friendliness of the different MC tools can be addressed in several ways. In-house developed solutions for MC engines have tried to make the process as automatic as possible, thus requiring less user interaction (for example, [86, 172]). These solutions may not be specifically designed for treatment monitoring prediction. However, they give insights regarding what can be done to make complex codes and tools more widespread and easy to use even for the less information technology-savvy clinical staff members.

More general solutions can be found in the derivatives from the general-purpose MC tools, for which the Geant4-based ecosystem is a prime example. Geant4 is written in C++, often considered a more complex programming language than others. Ideally, the programming language in which a tool for clinical applications is written should be irrelevant since the clinical staff should be provided with a tool agnostic of its inner workings. Unfortunately, in emerging technologies such as PG imaging, the situation may be like the egg and chicken scenario where no user-friendly tools are developed because there is no widespread PG imaging, and there is no widespread PG imaging partially due to the non-existence of software tools to exploit it. Therefore, how accessible general-purpose MC tools like Geant4 and its derivatives are matters when the community is at a stage of proving the usefulness of PG imaging. In this context, the Geant4 developers already had in mind a feature implemented in the code base to assist in developing solutions that people could use with barely any programming knowledge: they call such a feature a messenger class. In layperson's terms, a messenger is a type of class responsible for parsing a text file, and, based on expected text entries written in that text file, it executes the predefined set of instructions. Compare the two cases below to create an isotropic point photon source using the default Geant4 particle gun (see listing 1) and the General Particle Source (GPS, see listing 2), which relies heavily on the usage of English-based text commands.

Listing 1 Example of how to create an isotropic point photon source using the default Geant4 particle gun.

```
// Code adapted from the Geant4 example TestEm4 - version Geant4 11.2

// Find and define a photon as primary
G4ParticleDefinition* particle =
        G4ParticleTable::GetParticleTable()->FindParticle("gamma");
fParticleGun->SetParticleDefinition(particle);

// Energy of the photons
fParticleGun->SetParticleEnergy( 9.0*MeV );

// Initial position of the photons
fParticleGun->SetParticlePosition(G4ThreeVector( 0.*cm, 0.*cm, 0.*cm) );

// Randomize the direction cosines to define an isotropic emission
G4double cosTheta = 2*G4UniformRand() - 1., phi = twopi*G4UniformRand();
G4double sinTheta = std::sqrt(1. - cosTheta*cosTheta);
G4double px = sinTheta*std::cos(phi);
G4double py = sinTheta*std::sin(phi);
G4double pz = cosTheta;
fParticleGun->SetParticleMomentumDirection( G4ThreeVector(px, py, pz) );
```

Listing 2 Example of how to create an isotropic point photon source using GPS in a macro file.

```
# Define a photon as primary
/gps/particle gamma

# Define a point source
/gps/pos/type Point

# Energy of the photons
/gps/ene/mono 9.0 MeV

# Isotropic emission
/gps/ang/type iso

# Initial position of the photons
/gps/pos/centre 0 0 0 m
```

Such an approach of using input text files, also known as macro files, to define the entire simulation properties (geometry, physics models, source, scoring and scoring postprocessing) is behind, if not all, at least most of Geant4 derivatives. In the field of particle therapy, GATE [50], GAMOS [6] and TOPAS [113] are especially noteworthy due to their adoption. In turn, instead of text-based input files, the FLUKA MC tool [29] is associated with a graphical user interface called Flair [173], which avoids the usage of Fortran for many of the tasks required to define the parameters for an MC simulation, hence replacing Fortran programming with an intuitive, primarily point-and-click and input the required values, workflow.

Improving the user-friendliness of the different tools does not solve the issue of computational time. PG emission is derived from nuclear interactions, and those are known for their computational demands. Speeding up the interaction modelling of the stages of a nuclear reaction is rather complex unless more simplified hadronic models are used. Furthermore, parallelisation, namely employing general-purpose computing on graphics processing units (GPGPU), is challenging primarily because of divergence in the code execution that prevents full exploitation of the GPGPU (each parallel thread dealing with the nuclear interaction modelling is doing something different). There are many implementations of GPGPU MC-based dose calculation engines for particle therapy in the literature. Two examples are [51, 82]. However, hadronic interactions are typically not explicitly modelled but instead relevant quantities sampled from simplified models or cross-section databases (for example, [130]). An exception is the work of Tseung and Beltran [174] where the authors implemented an intranuclear cascade and evaporation simulation in GPGPU, and a follow-up study where the hadronic interactions were included in a fast GPGPU Monte Carlo code for proton therapy dose calculations [175]. From an implementation point of view, the simulation of PG emission does not require explicit nuclear interaction modelling. Suppose the cross-sections for each reaction of interest and material are known. In that case, estimating PG emission is trivial when propagating an ion through the medium and using the ion energy at each step, as it was done, for example, in Verburg *et al.* [172] or Sterpin *et al.* [153]. However, it was also shown by Verburg *et al.* [170] that cross-section databases may not necessarily be the most accurate source of data. Noteworthy examples of fast MC tools employed in proton therapy are MCsquare [151] and FRED [143], and goCMC [130], MonteRay [81] and FRED [143] as fast MC-based dose engines for carbon ion therapy.

An alternative approach is to explore variance reduction techniques. El Kanawati *et al.* [54] proposed a dedicated variance reduction technique for PG emission based on a track-length estimator. The authors reported efficiency gains in the order of 10^5. A follow-up study from Huisman *et al.* [45] improved the work of El Kanawati [54] by extending it to voxelised volumes, hence allowing for simulation in patient CT images.

6.2 Analytical approaches

Analytical approaches may not offer the accuracy and flexibility of MC tools. However, similarly to the pencil beam algorithm having its place in particle therapy, the prediction of PG distributions using analytical tools may have its place, too. MC tools, even the fast ones, may still be too slow or difficult to maintain. Furthermore, as discussed in section 5, MC tools can deliver significantly inaccurate results for PG radiation modelling. It must be stressed that the analytical approaches discussed below use MC data for their development. The usage of MC data implies that any inaccuracy therein will likely be, at least partially, imparted into the analytical approach. Therefore, the developers and users of such approaches should be aware of this fact. However, analytical approaches might be easier to tweak with experimentally-driven ad-hoc adjustments than tailoring an MC tool with its extensive, generalised and often complex code to reproduce experimental data.

The first analytical approach relevant to PG imaging to mention is the one behind PG distribution prediction when using a knife-edge slit camera, which is based on the work of Sterpin *et al*. [154]. The authors built a database of PG distributions per target nuclei using MC simulations. This database of PG distributions is employed to estimate the emission per CT voxel using a raytracing algorithm along the beam axis. When associating a PG emission yield with a voxel, the value is weighted by the fraction of the target nuclei in the voxel. To emulate the size of the spot and lateral distribution of PG, the authors use a Gaussian-weighted method to distribute the PG emission perpendicularly to the beam axis. The energy of the proton is calculated based on a continuous slowing-down approximation (CSDA), which in turn is used to estimate the PG energy spectrum per voxel in the range of 3–8 MeV based on the PG emission cross-sections differential in the energy of International Commission on Radiation Units and Measurements (ICRU) report 63 [48]. In the same workflow, Sterpin *et al*. also modelled the camera response using MC simulations. They created a transfer function that can be used to estimate the camera response for the PG emission predicted by their analytical approach [154]. This elegant solution allows for the prediction of the PG emission and the prediction of the detected signal in the same software solution. This prediction solution was integrated into the OpenReggui package (https://openreggui.org/), which enables the usage of the prediction tools in a clinically oriented environment where Digital Imaging and Communications in Medicine (DICOM) files input/output, picture archiving and communication system (PACS) access, image registration, MC dose calculation, and cone-beam CT (CBCT) reconstruction co-exist in the same platform.

The second analytical approach to mention is the so-called filtering approach. Parodi and Bortfeld [107] created a mathematical framework based on the following premise: there must exist a function that convolved with dose yields a positron emitter (PE) distribution. Due to its resemblance to convolution filters (kernels) usage, the authors coined the method as the filtering approach. They demonstrated that such a function exists and can be obtained from the convolution of a Gaussian with a power-law function, known as a $\tilde{Q}_v$ function. The authors were focused on PET monitoring when they proposed this method. It had a constraint, though: the method is only meaningful to be considered if the filtering approach exhibits energy invariance, i.e. the relationship between PE distribution and dose distribution does not change significantly so that the method can be employed in the entire clinical energy range. The approach could still be used if strong energy dependency is observed. However, that would require multiple filter functions, probably even one filter function per energy, which would boil down this approach to a parameterisation of PE distributions per energy.

The usage of the filtering approach was reported several times after its initial proposal and invariably applied to PET monitoring [8, 32, 40, 110]. That changed in 2016 when Schumann [146] applied the filtering approach to PG monitoring for the first time. However, Schumann et al. did not have the PG prediction as an end goal: they used the filtering approach as a step in the workflow to achieve dose reconstruction using an evolutionary algorithm. Nevertheless, their work was the first to demonstrate the applicability of the filtering approach for homogeneous water phantoms in the context of PG imaging and with outstanding results [146]. More on dose reconstruction is discussed in section 7.

Pinto *et al*. [120] generalised the filtering approach to both PET and PG monitoring and integrated them into a research version of the commercial TPS RayStation. The filtering approach is particularly suitable to be integrated into a TPS because, when analysing the formalism of the pencil beam algorithm, it becomes evident that both dose and PE/PG distributions share the same governing quantity, the particle fluence spectrum [120]. The fact that both cases rely on the particle fluence spectrum allows for the exploitation of the entire TPS infrastructure, but rather than using laterally-integrated depth-dose profiles as input for the pencil beam algorithm, laterally-integrated depth-PE/PG profiles are utilised instead. Pinto *et al*. [120] also included a method based on look-up tables (LUT) to estimate the PG energy spectrum per CT voxel, which enables arbitrary energy selections, thus allowing for PG prediction of characteristic PG emission or a range of energies, such as 3–8 MeV for the knife-edge slit camera [154]. The PE and PG predictions using the filtering approach were benchmarked against full-blown MC simulations (PE was additionally benchmarked against clinical offline PET monitoring images) [120], and comparison of PG prediction against measured PG data is ongoing. Figure 15 depicts the comparison of MC and TPS for dose, PE and PG for four patients.

An advantage of the solution developed by Pinto *et al*. [120] is the direct implementation in the TPS. Such an implementation allows for the highest level of clinical workflow integration possible. The same software where the clinical staff optimises and assesses treatment plans, prepares dosimetry QA, and evaluates patient alignment (for example, using digitally reconstructed radiograph (DRR) registration) is also used to calculate and review the expected PET and PG images if the plan is adequately delivered to the patient. Figure 16 depicts the PG prediction module, the RayStation GUI with the dose, and the PE and PG predictions.

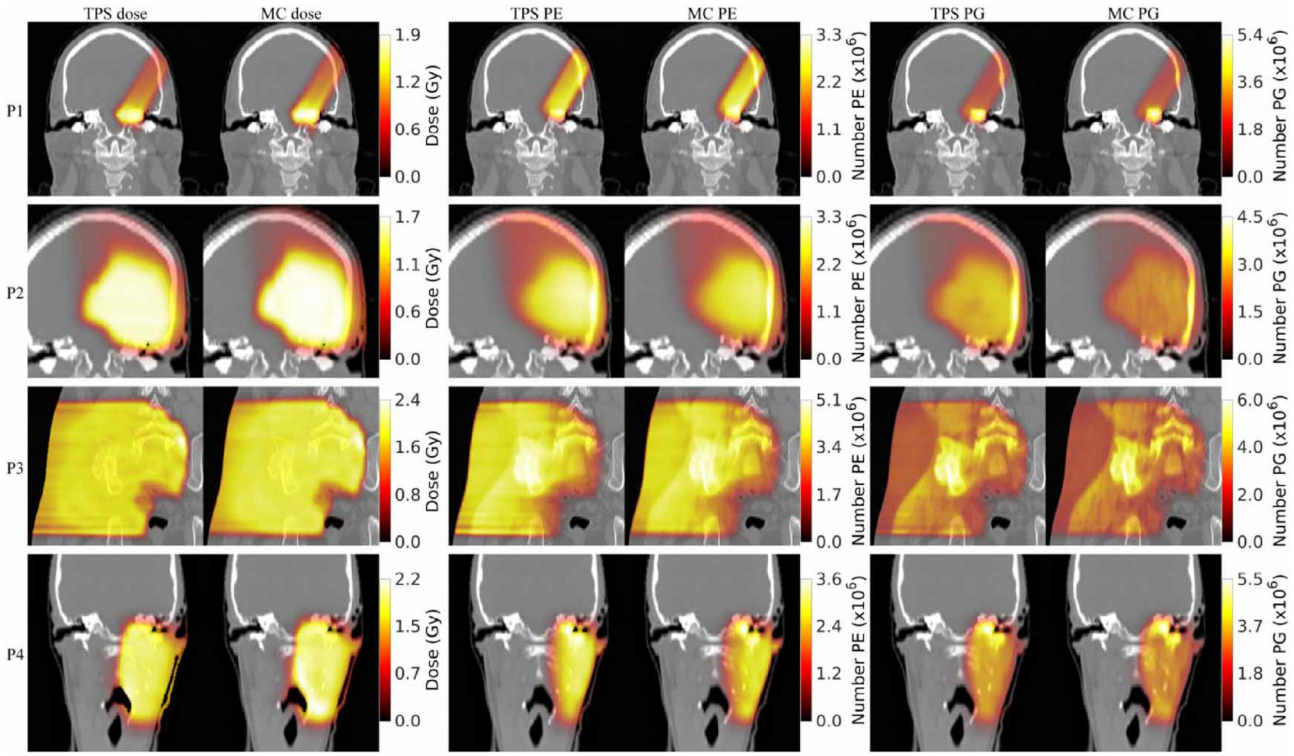

Fig. 15 Comparison of distributions (dose, PE and PG from left to right) between TPS and MC distributions for all patients (P1 to P4 from top to bottom). Reproduced from [120] under the terms of the Creative Commons Attribution 3.0 licence (CC BY, https://creativecommons.org/licenses/by/3.0/)

Even though the clinical use of the filtering PG module in RayStation has not been reported so far, the PET module has been under intensive usage at the Shanghai Proton and Heavy Ion Center (SPHIC), and clinical research exploiting the solution developed by Pinto *et al*. [120] has been published [184, 185].

6.3 Machine learning

Machine learning is routinely used in PG imaging for data analysis and selection. It is an approach widely employed in Compton camera studies to assist in identifying good events (for example, [9, 10, 52, 59, 71]). However, machine learning-based solutions still need to be proposed to predict PG distributions and intense research is ongoing. The approach is quite appealing: using the treatment plan and the CT as input and an artificial intelligence model will immediately predict the PG distributions. Such an approach could be a compelling alternative to analytical approaches.

Nevertheless, if the PET monitoring experience shows anything, those dedicated PG solutions will be developed and published sooner or later. An introduction and discussion on using machine learning approaches for predicting and exploiting PET monitoring images are outside this manuscript's scope. However, such applications can be found in the literature (for example, [72, 75, 83]).

7 Translation into clinical applications

The best example of translational research employing PG imaging is currently being done at OncoRay and University Proton Therapy Dresden (UPTD, Dresden, Germany). This team was the first to use the knife-edge slit camera for PG imaging in 2016 [134], and since then, they have expanded its application and improved workflows. Their world-class work gives a glimpse of how PG imaging can greatly impact the future of proton therapy. In their optimised workflows, the impact of using PG imaging to monitor the treatment of a patient is minor: it implies adding one extra minute per field to the total irradiation duration for positioning the knife-edge slit camera trolley [15]. Pietsch *et al*. [116] developed automatic detection and classification tools to assess treatment deviations in proton therapy using realistically simulated PG imaging data on twelve head-and-neck cancer patients. The authors applied convolutional neural networks and conventional machine-learning approaches on 386 investigated scenarios resembling relevant or non-relevant treatment deviations simulated on planning and control CTs. They found that convolutional neural networks could detect treatment deviations and identify their source (setup error, range prediction errors, or anatomical changes by CT voxel manipulation) with good performance. A breakthrough follow-up study was reported soon after, with some of the tools and lessons derived from

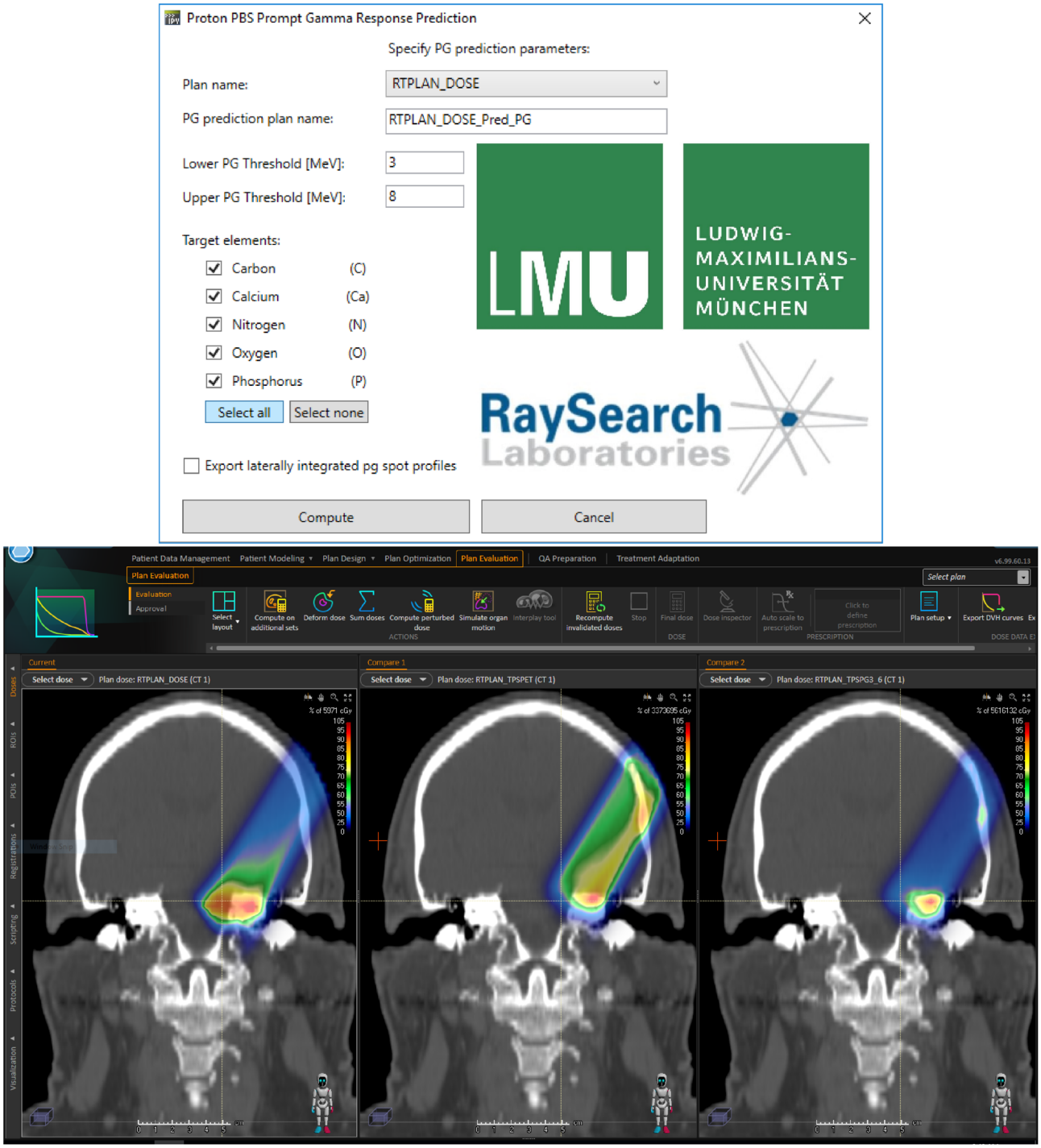

Fig. 16 Top: graphical user interface of the PG prediction module where the user can select the target nuclei and the energy range for PG prediction. Bottom: graphical user interface of the RayStation research version used with the dose (left), PE (middle) and PG (right) predictions. The CT slice, dose, and prediction data in this figure are the same as in Fig. 15, top row (patient P1), but shown in RayStation as it would be likely used in a clinical setting. For details refer to Pinto *et al*. [120]

Pietsch *et al*. [116] being used in the PG-based monitoring of 15 prostate cancer patients [14] treated at the University Proton Therapy Dresden (UPTD) centre. In this study, PG imaging measurements were performed during 105 fractions, corresponding to 201 fields, assisted by acquiring CT images using the in-room control CT scanner. The authors were able to demonstrate evidence of the detection capability of anatomical changes in prostate cancer patients undergoing proton therapy using clinically acquired PG imaging data [14]. Finally, the OncoRay team also published a study that arguably may have the most striking implications for the future of proton therapy: testing the reduction of range uncertainty margins when using PG imaging [15]. Bertschi *et al*.

[15] compared a reference case to cases with margin reduction when using PG imaging-based monitoring alone (case 1), and when using PG imaging-based monitoring and volumetric imaging for setup (in-room CT scanner, case 2). The reference case considers a patient setup uncertainty margin of 3 mm and a range uncertainty margin of 7 mm, while case 1 uses 3 mm and 3 mm (−57%) and case 2 utilises 1 mm (−67%) and 3 mm (−57%), respectively. For the clinical cases studied, the authors demonstrated that the margin reductions related to range uncertainty (from 7 to 3 mm) had a more significant effect on reducing the mean dose in surrounding healthy tissue than the margin reduction allowed by the volumetric imaging for setup.

An exciting translation into clinical applications is dose reconstruction. Dose reconstruction aims to obtain the dose distributions delivered to the patient using particle therapy monitoring information. The rationale for dose reconstruction is straightforward: clinical staff in a particle therapy centre primarily work with (physical and biological) dose distributions and increasingly more with LET distributions. Adding another layer of complexity by introducing the analysis of PG distributions in the clinical workflow might hinder the adoption of PG imaging, namely when the PG distributions cannot be directly compared to dose ones and require a chain of tools to conclude on treatment delivery quality. A robust, fast and accurate algorithm for dose reconstruction based on PG imaging could pave the way for a smoother transition of PG-based solutions into clinical practice. Nevertheless, it must be said that the work of excellence reported from OncoRay and UPTD also shows that dose reconstruction algorithms are not mandatory to accomplish clinical implementations that ultimately benefit patients.

In PET monitoring applications, such a dose reconstruction concept has been subject to extensive research, for example, [41, 90, 131, 140]. In the case of PG-based monitoring, Schumann *et al*. [146] was the first report of dose reconstruction using PG imaging. Therein, an evolutionary algorithm was used coupled with the filtering approach, and the authors demonstrated the feasibility of performing PG-based dose reconstruction in homogeneous water phantoms for both pencil beams and spread-out Bragg peaks (SOBP). In turn, Liu and Huang [74] relied on deep-learning approaches to accomplish the dose reconstruction. Mean Bragg peak position errors of less than 0.4 mm were observed when considering different simulation conditions. However, the authors also realised that the developed approach required high-quality PG images, and there are challenges when dealing with PG images with low counts or with limited spatial resolution [74]. Finally, one of the projects of the Real-Time Adaptive Particle Therapy Of Cancer (RAPTOR) consortium (https://raptor-consortium.com/) is tackling the dose reconstruction problem from a practical point of view, *i.e*. not only developing methods that can perform PG-based dose reconstruction but also assessing which methods are the most likely candidates to be deployed in a clinical setting due to, for example, accuracy, robustness, computation time or usage complexity.

8 The future of PG imaging

The future of PG imaging looks bright. The quantity of research on this topic is overwhelming, considering the number of particle therapy centres worldwide. In the past years, a considerable amount of research has been devoted to reducing treatment uncertainties by exploring different imaging modalities and protocols.

Proton CT can reduce imaging uncertainties by imaging the patient with the same radiation quality as the one used for treatment, which means that radiation interaction in the patient's body will be the same, albeit at higher energies. This radiation quality equivalence leads imaging contrasts to relate closely to the quantity of interest, the relative stopping power [125]. Direct assessment of relative stopping powers via proton imaging could give more accuracy on relative stopping power estimation [25] while delivering the same or less imaging dose to the patients [144]. A competing approach to proton CT in order to estimate more accurate relative stopping powers than conventional CT is dual-energy CT [25] or spectral CT [79].

Imaging protocols can also contribute to the reduction of patient setup uncertainties. Better usage of CBCT techniques or in-room CT that can be used to assist in patient setup and positioning. The highest level of accuracy and precision using the in-room CT occurs when coupled with robotic structures to transfer the patient from imaging to treatment and vice versa. Such approaches allow for a high degree of reduction in safety margins associated with the patient setup. As mentioned in section 7, Bertschi *et al*. [15] reduced setup margins from 3 mm to 1 mm, a reduction of 67% by employing volumetric imaging for positioning. Alternatively, magnetic resonance imaging-guided (MRI-guided) proton therapy is a technique that, although still in its infancy, promises ionising radiation-free in-vivo and online image-guided proton therapy [39]. A preliminary investigation of an MRI-guided proton beamline has been presented recently at OncoRay [104, 142]. Insights on the usage of MRI-Linac machines relevant to the discussion herein point to significant inter-fractional and intra-fractional target position variations of the pancreas, prostate, and oesophagus [16, 68, 101, 104].

Nevertheless, none of the proposals that allow for better tissue modelling, better positioning or better anatomical assessment offers the possibility of in-vivo assessment of the actual dose delivered to the patient. All those approaches give the means for better dose estimation but do not ensure that such estimation was the actual dose delivered. Planning, setup and online anatomic (MRI, X-ray fluoroscopy [156] or proton radiography [36]) imaging modalities do reduce uncertainties and give higher levels of confidence that what was planned is what was delivered. Still, they do not provide information about where the dose was delivered. The benefits of using in-vivo online monitoring techniques, like PG-based monitoring, are clear: they give feedback on where the dose was delivered or, at the very least, if the ion ranges were, within some technique-related uncertainty, as expected.

Regardless of the benefits that PG imaging might bring, it is paramount to remember that it is not some sort of ion range uncertainty panacea. PG imaging is challenging and full of obstacles that must be overcome, from unfavourable physics (low PG

radiation yields) to integration into the clinical workflow. For anyone who has ever worked in the PG imaging field, this is a lesson that is not easily forgotten.

Adaptive radiotherapy protocols, or the more demanding online radiotherapy protocols, let the treatment plan be adapted for each patient depending on their unique circumstances in the progress of their radiotherapy treatment [73, 99, 104, 181]. In-vivo range monitoring approaches may hold the key to achieving the highest level of QA in an adaptive radiotherapy protocol, and it is no surprise that the mounting of PG imaging devices in the treatment gantry is being considered [15]. With the increasing interest in adaptive radiotherapy protocols, PG imaging will likely take a central role in fulfilling the dream behind adaptive radiotherapy: fully bringing personalised, precise medicine approaches into particle therapy.

Funding Open Access funding enabled and organized by Projekt DEAL.

Data Availability Statement No data associated in the manuscript.

Declarations

Conflict of interest The author declares the following financial interests/personal relationships, which may be considered potential. LMU has a research collaboration agreement with RaySearch Laboratories AB. The author received no financial support in the writing of this publication.

References

1. C. Agodi, F. Bellini, G.A.P. Cirrone, F. Collamati, G. Cuttone, E.D. Lucia, M.D. Napoli, A.D. Domenico, R. Faccini, F. Ferroni, S. Fiore, P. Gauzzi, E. Iarocci, M. Marafini, I. Mattei, A. Paoloni, V. Patera, L. Piersanti, F. Romano, A. Sarti, A. Sciubba, C. Voena, Precise measurement of prompt photon emission from 80 MeV/u carbon ion beam irradiation. J. Instrum. **7**(03), 03001 (2012). https://doi.org/10.1088/1748-0221/7/03/P03001
2. S. Agostinelli, J. Allison, K. Amako, J. Apostolakis, H. Araujo, P. Arce, M. Asai, D. Axen, S. Banerjee, G. Barrand, F. Behner, L. Bellagamba, J. Boudreau, L. Broglia, A. Brunengo, H. Burkhardt, S. Chauvie, J. Chuma, R. Chytracek, G. Cooperman, G. Cosmo, P. Degtyarenko, A. Dell'Acqua, G. Depaola, D. Dietrich, R. Enami, A. Feliciello, C. Ferguson, H. Fesefeldt, G. Folger, F. Foppiano, A. Forti, S. Garelli, S. Giani, R. Giannitrapani, D. Gibin, J.J. Gómez Cadenas, I. González, G. Gracia Abril, G. Greeniaus, W. Greiner, V. Grichine, A. Grossheim, S. Guatelli, P. Gumplinger, R. Hamatsu, K. Hashimoto, H. Hasui, A. Heikkinen, A. Howard, V. Ivanchenko, A. Johnson, F.W. Jones, J. Kallenbach, N. Kanaya, M. Kawabata, Y. Kawabata, M. Kawaguti, S. Kelner, P. Kent, A. Kimura, T. Kodama, R. Kokoulin, M. Kossov, H. Kurashige, E. Lamanna, T. Lampén, V. Lara, V. Lefebure, F. Lei, M. Liendl, W. Lockman, F. Longo, S. Magni, M. Maire, E. Medernach, K. Minamimoto, P. Mora de Freitas, Y. Morita, K. Murakami, M. Nagamatu, R. Nartallo, P. Nieminen, T. Nishimura, K. Ohtsubo, M. Okamura, S. O'Neale, Y. Oohata, K. Paech, J. Perl, A. Pfeiffer, M.G. Pia, F. Ranjard, A. Rybin, S. Sadilov, E. Di Salvo, G. Santin, T. Sasaki, N. Savvas, Y. Sawada, S. Scherer, S. Sei, V. Sirotenko, D. Smith, N. Starkov, H. Stoecker, J. Sulkimo, M. Takahata, S. Tanaka, E. Tcherniaev, E. Safai Tehrani, M. Tropeano, P. Truscott, H. Uno, L. Urban, P. Urban, M. Verderi, A. Walkden, W. Wander, H. Weber, J.P. Wellisch, T. Wenaus, D.C. Williams, D. Wright, T. Yamada, H. Yoshida, D. Zschiesche, Geant4-a simulation toolkit. Nucl. Instrum. Methods Phys. Res., Sect. A **506**(3), 250–303 (2003). https://doi.org/10.1016/S0168-9002(03)01368-8
3. S. Aldawood, P.G. Thirolf, A. Miani, M. Böhmer, G. Dedes, R. Gernhäuser, C. Lang, S. Liprandi, L. Maier, T. Marinšek, M. Mayerhofer, D.R. Schaart, I.V. Lozano, K. Parodi, Development of a compton camera for prompt-gamma medical imaging. Radiat. Phys. Chem. **140**, 190–197 (2017). https://doi.org/10.1016/j.radphyschem.2017.01.024. (**2nd International Conference on Dosimetry and its Applications (ICDA-2) University of Surrey, Guildford, United Kingdom, 3-8 July 2016**)
4. U. Amaldi, G. Kraft, Radiotherapy with beams of carbon ions. Rep. Prog. Phys. **68**(8), 1861 (2005). https://doi.org/10.1088/0034-4885/68/8/R04
5. C. Ammar, K. Frey, J. Bauer, C. Melzig, S. Chiblak, M. Hildebrandt, D. Unholtz, C. Kurz, S. Brons, J. Debus, A. Abdollahi, K. Parodi, Comparing the biological washout of β+-activity induced in mice brain after 12C-ion and proton irradiation. Phys. Med. Biol. **59**(23), 7229 (2014). https://doi.org/10.1088/0031-9155/59/23/7229
6. P. Arce, J.I. Lagares, L. Harkness, L. Desorgher, G. Lorenzo, Y. Abreu, Z. Wang, GAMOS: An easy and flexible way to use GEANT4. In: 2011 IEEE Nuclear Science Symposium Conference Record, pp. 2230–2237 (2011). https://doi.org/10.1109/NSSMIC.2011.6154455
7. W. Assmann, S. Kellnberger, S. Reinhardt, S. Lehrack, A. Edlich, P.G. Thirolf, M. Moser, G. Dollinger, M. Omar, V. Ntziachristos, K. Parodi, Ionoacoustic characterization of the proton bragg peak with submillimeter accuracy. Med. Phys. **42**(2), 567–574 (2015). https://doi.org/10.1118/1.4905047
8. F. Attanasi, A. Knopf, K. Parodi, H. Paganetti, T. Bortfeld, V. Rosso, A. Del Guerra, Extension and validation of an analytical model for in vivo PET verification of proton therapy-a phantom and clinical study. Phys. Med. Biol. **56**(16), 5079–98 (2011). https://doi.org/10.1088/0031-9155/56/16/001
9. J. Balibrea-Correa, J. Lerendegui-Marco, V. Babiano-Suarez, C. Domingo-Pardo, I. Ladarescu, C. Guerrero, T. Rodríguez-González, M.C. Jiménez-Ramos, Hadron therapy range verification via machine-learning aided prompt-gamma imaging. In: 2021 IEEE Nuclear Science Symposium and Medical Imaging Conference (NSS/MIC), pp. 1–7 (2021). https://doi.org/10.1109/NSS/MIC44867.2021.9875637
10. C.A. Barajas, G.C. Kroiz, M.K. Gobbert, J.C. Polf, Classification of compton camera based prompt gamma imaging for proton radiotherapy by random forests. In: 2021 International Conference on Computational Science and Computational Intelligence (CSCI), pp. 308–311 (2021). https://doi.org/10.1109/CSCI54926.2021.00124
11. L. Barrientos, M. Borja-Lloret, A. Etxebeste, E.M. Noz, J.F. Oliver, A. Ros, J. Roser, C. Senra, R. Viegas, G. Llosá, Performance evaluation of MACACO II Compton camera. Nucl. Instrum. Methods Phys. Res., Sect. A **1014**, 165702 (2021). https://doi.org/10.1016/j.nima.2021.165702
12. L. Barrientos, M. Borja-Lloret, J.V.C. Na, P. Dendooven, J. García López, F. Hueso-González, M.C. Jiménez-Ramos, J. Pérez-Curbelo, A. Ros, J. Roser, C. Senra, R. Viegas, G. Llosá, Gamma-ray sources imaging and test-beam results with MACACO III Compton camera. Phys. Med. **117**, 103199 (2024). https://doi.org/10.1016/j.ejmp.2023.103199

13. J. Bauer, D. Unholtz, F. Sommerer, C. Kurz, T. Haberer, K. Herfarth, T. Welzel, S.E. Combs, J. Debus, K. Parodi, Implementation and initial clinical experience of offline PET/CT-based verification of scanned carbon ion treatment. Radiother. Oncol. **107**(2), 218–226 (2013). https://doi.org/10.1016/j.radonc.2013.02.018
14. J. Berthold, J. Pietsch, N. Piplack, C. Khamfongkhruea, J. Thiele, T. Hölscher, G. Janssens, J. Smeets, E. Traneus, S. Löck, K. Stützer, C. Richter, Detectability of anatomical changes with prompt-gamma imaging: first systematic evaluation of clinical application during prostate-cancer proton therapy. Int. J. Radiat. Oncol. Biol. Phys. **117**(3), 718–729 (2023). https://doi.org/10.1016/j.ijrobp.2023.05.002
15. S. Bertschi, K. Stützer, J. Berthold, J. Pietsch, J. Smeets, G. Janssens, C. Richter, Potential margin reduction in prostate cancer proton therapy with prompt gamma imaging for online treatment verification. Phys. Imaging Radiat. Oncol. (2023). https://doi.org/10.1016/j.phro.2023.100447
16. M.R. Boekhoff, I.L. Defize, A.S. Borggreve, N. Takahashi, A.L.H.M.W. van Lier, J.P. Ruurda, R. van Hillegersberg, J.J.W. Lagendijk, S. Mook, G.J. Meijer, 3-dimensional target coverage assessment for mri guided esophageal cancer radiotherapy. Radiother. Oncol. **147**, 1–7 (2020). https://doi.org/10.1016/j.radonc.2020.03.007
17. V. Bom, L. Joulaeizadeh, F. Beekman, Real-time prompt gamma monitoring in spot-scanning proton therapy using imaging through a knife-edge-shaped slit. Phys. Med. Biol. **57**(2), 297 (2011). https://doi.org/10.1088/0031-9155/57/2/297
18. T. Bowen, Radiation-induced thermoacoustic soft tissue imaging. In: 1981 Ultrasonics Symposium, pp. 817–822 (1981). https://doi.org/10.1109/ULTSYM.1981.197737
19. J.L. Cantley, C.-W. Cheng, F.B. Jesseph, T.K. Podder, V.C. Colussi, B.J. Traughber, L.E. Ponsky, R.J. Ellis, Real-time in vivo dosimetry for sbrt prostate treatment using plastic scintillating dosimetry embedded in a rectal balloon: a case study. J. Appl. Clin. Med. Phys. **17**(6), 305–311 (2016). https://doi.org/10.1120/jacmp.v17i6.6508
20. W. Chen, J. Unkelbach, A. Trofimov, T. Madden, H. Kooy, T. Bortfeld, D. Craft, Including robustness in multi-criteria optimization for intensity-modulated proton therapy. Phys. Med. Biol. **57**(3), 591 (2012). https://doi.org/10.1088/0031-9155/57/3/591
21. H.J. Choi, J.W. Jang, W.-G. Shin, H. Park, S. Incerti, C.H. Min, Development of integrated prompt gamma imaging and positron emission tomography system for in vivo 3-D dose verification: a Monte Carlo study. Phys. Med. Biol. **65**(10), 105005 (2020). https://doi.org/10.1088/1361-6560/ab857c
22. J. Clark, A. Gaillard, J. Koe, N. Navarathna, D.J. Kelly, M.K. Gobbert, C.A. Barajas, J.C. Polf, Multi-layer recurrent neural networks for the classification of compton camera based imaging data for proton beam cancer treatment. In: 2022 IEEE/ACM International Conference on Big Data Computing, Applications and Technologies (BDCAT), pp. 213–222 (2022). https://doi.org/10.1109/BDCAT56447.2022.00038
23. L. Cozzi, A. Fogliata, A. Lomax, A. Bolsi, A treatment planning comparison of 3D conformal therapy, intensity modulated photon therapy and proton therapy for treatment of advanced head and neck tumours. Radiother. Oncol. **61**(3), 287–297 (2001). https://doi.org/10.1016/S0167-8140(01)00403-0
24. G. Dedes, M. Pinto, D. Dauvergne, N. Freud, J. Krimmer, J.M. Létang, C. Ray, E. Testa, Assessment and improvements of geant4 hadronic models in the context of prompt-gamma hadrontherapy monitoring. Phys. Med. Biol. **59**(7), 1747 (2014). https://doi.org/10.1088/0031-9155/59/7/1747
25. G. Dedes, J. Dickmann, K. Niepel, P. Wesp, R.P. Johnson, M. Pankuch, V. Bashkirov, S. Rit, L. Volz, R.W. Schulte, G. Landry, K. Parodi, Experimental comparison of proton CT and dual energy x-ray CT for relative stopping power estimation in proton therapy. Phys. Med. Biol. **64**(16), 165002 (2019). https://doi.org/10.1088/1361-6560/ab2b72
26. E. Draeger, D. Mackin, S. Peterson, H. Chen, S. Avery, S. Beddar, J.C. Polf, 3D prompt gamma imaging for proton beam range verification. Phys. Med. Biol. **63**(3), 035019 (2018). https://doi.org/10.1088/1361-6560/aaa203
27. M. Engelsman, M. Schwarz, L. Dong, Physics controversies in proton therapy. Semin. Radiat. Oncol. **23**(2), 88–96 (2013). https://doi.org/10.1016/j.semradonc.2012.11.003. (**Controversies in Proton Therapy**)
28. F.S. Englbrecht, S. Trinkl, V. Mares, W. Rühm, M. Wielunski, J.J. Wilkens, M. Hillbrand, K. Parodi, A comprehensive Monte Carlo study of out-of-field secondary neutron spectra in a scanned-beam proton therapy gantry room. Z. Med. Phys. **31**(2), 215–228 (2021). https://doi.org/10.1016/j.zemedi.2021.01.001
29. A. Ferrari, P.R. Sala, A. Fasso, J. Ranft, FLUKA: a multi-particle transport code (2005). CERN-2005-10, INFN/TC_05/11, SLAC-R-773
30. V. Ferrero, P. Cerello, E. Fiorina, V. Monaco, M. Rafecas, R. Wheadon, F. Pennazio, Innovation in online hadrontherapy monitoring: an in-beam pet and prompt-gamma-timing combined device. Nucl. Instrum. Methods Phys. Res., Sect. A **936**, 48–49 (2019). https://doi.org/10.1016/j.nima.2018.08.065. (**Frontier Detectors for Frontier Physics: 14th Pisa Meeting on Advanced Detectors**)
31. M. Fontana, J.-L. Ley, D. Dauvergne, N. Freud, J. Krimmer, J.M. Létang, V. Maxim, M.-H. Richard, I. Rinaldi, E. Testa, Monitoring ion beam therapy with a compton camera: simulation studies of the clinical feasibility. IEEE Trans. Radiat. Plasma Med. Sci. **4**(2), 218–232 (2020). https://doi.org/10.1109/TRPMS.2019.2933985
32. K. Frey, J. Bauer, D. Unholtz, C. Kurz, M. Kramer, T. Bortfeld, K. Parodi, TPS(PET)-a TPS-based approach for in vivo dose verification with PET in proton therapy. Phys. Med. Biol. **59**(1), 1–21 (2014). https://doi.org/10.1088/0031-9155/59/1/1
33. M.F. Gensheimer, T.I. Yock, N.J. Liebsch, G.C. Sharp, H. Paganetti, N. Madan, P.E. Grant, T. Bortfeld, In vivo proton beam range verification using spine MRI changes. Int. J. Radiat. Oncol. *Biol. *Phys. **78**(1), 268–275 (2010). https://doi.org/10.1016/j.ijrobp.2009.11.060
34. C. Golnik, F. Hueso-González, A. Müller, P. Dendooven, W. Enghardt, F. Fiedler, T. Kormoll, K. Roemer, J. Petzoldt, A. Wagner, G. Pausch, Range assessment in particle therapy based on prompt γ-ray timing measurements. Phys. Med. Biol. **59**(18), 5399 (2014). https://doi.org/10.1088/0031-9155/59/18/5399
35. P. Gueth, D. Dauvergne, N. Freud, J.M. Létang, C. Ray, E. Testa, D. Sarrut, Machine learning-based patient specific prompt-gamma dose monitoring in proton therapy. Phys. Med. Biol. **58**(13), 4563 (2013). https://doi.org/10.1088/0031-9155/58/13/4563
36. B. Han, X.G. Xu, G.T.Y. Chen, Proton radiography and fluoroscopy of lung tumors: a Monte Carlo study using patient-specific 4DCT phantoms. Med. Phys. **38**(4), 1903–1911 (2011). https://doi.org/10.1118/1.3555039
37. S. Helmbrecht, W. Enghardt, K. Parodi, B. Didinger, J. Debus, D. Kunath, M. Priegnitz, F. Fiedler, Analysis of metabolic washout of positron emitters produced during carbon ion head and neck radiotherapy. Med. Phys. **40**(9), 091918 (2013). https://doi.org/10.1118/1.4818424
38. P. Henriquet, E. Testa, M. Chevallier, D. Dauvergne, G. Dedes, N. Freud, J. Krimmer, J.M. Létang, C. Ray, M.-H. Richard, F. Sauli, Interaction vertex imaging (IVI) for carbon ion therapy monitoring: a feasibility study. Phys. Med. Biol. **57**(14), 4655 (2012). https://doi.org/10.1088/0031-9155/57/14/4655
39. A. Hoffmann, B. Oborn, M. Moteabbed, S. Yan, T. Bortfeld, A. Knopf, H. Fuchs, D. Georg, J. Seco, M.F. Spadea, O. Jäkel, C. Kurz, K. Parodi, MR-guided proton therapy: a review and a preview. Radiat. Oncol. **15**(1), 129 (2020). https://doi.org/10.1186/s13014-020-01571-x
40. T. Hofmann, A. Fochi, K. Parodi, M. Pinto, Prediction of positron emitter distributions for range monitoring in carbon ion therapy: an analytical approach. Phys. Med. Biol. **64**(10), 105022 (2019). https://doi.org/10.1088/1361-6560/ab17f9
41. T. Hofmann, M. Pinto, A. Mohammadi, M. Nitta, F. Nishikido, Y. Iwao, H. Tashima, E. Yoshida, A. Chacon, M. Safavi-Naeini, A. Rosenfeld, T. Yamaya, K. Parodi, Dose reconstruction from PET images in carbon ion therapy: a deconvolution approach. Phys. Med. Biol. **64**(2), 025011 (2019). https://doi.org/10.1088/1361-6560/aaf676
42. W.C. Hsi, M. Fagundes, O. Zeidan, E. Hug, N. Schreuder, Image-guided method for TLD-based in vivo rectal dose verification with endorectal balloon in proton therapy for prostate cancer. Med. Phys. **40**(5), 051715 (2013). https://doi.org/10.1118/1.4801901

43. F. Hueso-González, W. Enghardt, F. Fiedler, C. Golnik, G. Janssens, J. Petzoldt, D. Prieels, M. Priegnitz, K.E. Römer, J. Smeets, F.V. Stappen, A. Wagner, G. Pausch, First test of the prompt gamma ray timing method with heterogeneous targets at a clinical proton therapy facility. Phys. Med. Biol. **60**(16), 6247 (2015). https://doi.org/10.1088/0031-9155/60/16/6247
44. F. Hueso-González, M. Rabe, T.A. Ruggieri, T. Bortfeld, J.M. Verburg, A full-scale clinical prototype for proton range verification using prompt gamma-ray spectroscopy. Phys. Med. Biol. **63**(18), 185019 (2018). https://doi.org/10.1088/1361-6560/aad513
45. B.F.B. Huisman, J.M. Létang, E. Testa, D. Sarrut, Accelerated prompt gamma estimation for clinical proton therapy simulations. Phys. Med. Biol. **61**(21), 7725 (2016). https://doi.org/10.1088/0031-9155/61/21/7725
46. B.F.B. Huisman, E.M. Noz, D. Dauvergne, J.M. Létang, D. Sarrut, E. Testa, Analytical modeling and monte carlo simulations of multi-parallel slit and knife-edge slit prompt gamma cameras. Phys. Med. Biol. **68**(11), 115009 (2023). https://doi.org/10.1088/1361-6560/acd237
47. D. Hymers, E. Kasanda, V. Bildstein, J. Easter, A. Richard, A. Spyrou, C. Höhr, D. Mücher, Intra- and inter-fraction relative range verification in heavy-ion therapy using filtered interaction vertex imaging. Phys. Med. Biol. **66**(24), 245022 (2021). https://doi.org/10.1088/1361-6560/ac3b33
48. International Commission on Radiation Units and Measurements: Nuclear Data for Neutron and Proton Radiotherapy and for Radiation Protection (ICRUReport 63, 2000)
49. M. Jacquet, S. Marcatili, M.-L. Gallin-Martel, J.-L. Bouly, Y. Boursier, D. Dauvergne, M. Dupont, L. Gallin-Martel, J. Hérault, J.-M. Létang, D. Manéval, C. Morel, J.-F. Muraz, Testa: A time-of-flight-based reconstruction for real-time prompt-gamma imaging in proton therapy. Phys. Med. Biol. **66**(13), 135003 (2021). https://doi.org/10.1088/1361-6560/ac03ca
50. S. Jan, G. Santin, D. Strul, S. Staelens, K. Assié, D. Autret, S. Avner, R. Barbier, M. Bardiès, P.M. Bloomfield, D. Brasse, V. Breton, P. Bruyndonckx, I. Buvat, A.F. Chatziioannou, Y. Choi, Y.H. Chung, C. Comtat, D. Donnarieix, L. Ferrer, S.J. Glick, C.J. Groiselle, D. Guez, P.-F. Honore, S. Kerhoas-Cavata, A.S. Kirov, V. Kohli, M. Koole, M. Krieguer, D.J. Laan, F. Lamare, G. Largeron, C. Lartizien, D. Lazaro, M.C. Maas, L. Maigne, F. Mayet, F. Melot, C. Merheb, E. Pennacchio, J. Perez, U. Pietrzyk, F.R. Rannou, M. Rey, D.R. Schaart, C.R. Schmidtlein, L. Simon, T.Y. Song, J.-M. Vieira, D. Visvikis, R.V. Walle, E. Wieërs, C. Morel, GATE: a simulation toolkit for PET and SPECT. Phys. Med. Biol. **49**(19), 4543 (2004). https://doi.org/10.1088/0031-9155/49/19/007
51. X. Jia, J. Schümann, H. Paganetti, S.B. Jiang, GPU-based fast monte carlo dose calculation for proton therapy. Phys. Med. Biol. **57**(23), 7783 (2012). https://doi.org/10.1088/0031-9155/57/23/7783
52. Z. Jiang, J.C. Polf, C.A. Barajas, M.K. Gobbert, L. Ren, A feasibility study of enhanced prompt gamma imaging for range verification in proton therapy using deep learning. Phys. Med. Biol. **68**(7), 075001 (2023). https://doi.org/10.1088/1361-6560/acbf9a
53. Y. Jongen, F. Stichelbaut, Verification of the proton beam position in the patient by the prompt gamma rays emission. In: Abstracts of the 39th PTCOG Meeting. Particle Therapy Co-Operative Group
54. W.E. Kanawati, J.M. Létang, D. Dauvergne, M. Pinto, D. Sarrut, E. Testa, N. Freud, Monte carlo simulation of prompt γ-ray emission in proton therapy using a specific track length estimator. Phys. Med. Biol. **60**(20), 8067 (2015). https://doi.org/10.1088/0031-9155/60/20/8067
55. J. Kasper, K. Rusiecka, R. Hetzel, M.K. Kozani, R. Lalik, A. Magiera, A. Stahl, A. Wrońska, The sifi-cc project - feasibility study of a scintillation-fiber-based compton camera for proton therapy monitoring. Phys. Med. **76**, 317–325 (2020). https://doi.org/10.1016/j.ejmp.2020.07.013
56. L. Kelleter, A. Wrońska, J. Besuglow, A. Konefał, K. Laihem, J. Leidner, A. Magiera, K. Parodi, K. Rusiecka, A. Stahl, T. Tessonnier, Spectroscopic study of prompt-gamma emission for range verification in proton therapy. Phys. Med. **34**, 7–17 (2017). https://doi.org/10.1016/j.ejmp.2017.01.003
57. A.-C. Knopf, A. Lomax, In vivo proton range verification: a review. Phys. Med. Biol. **58**(15), 131 (2013). https://doi.org/10.1088/0031-9155/58/15/R131
58. T. Kormoll, F. Fiedler, S. Schöne, J. Wüstemann, K. Zuber, W. Enghardt, A compton imager for in-vivo dosimetry of proton beams - a design study. Nucl. Instrum. Methods Phys. Res., Sect. A **626–627**, 114–119 (2011). https://doi.org/10.1016/j.nima.2010.10.031
59. M.K. Kozani, Machine learning approach for proton range verification using real-time prompt gamma imaging with compton cameras: addressing the total deposited energy information gap. Phys. Med. Biol. **69**(7), 075019 (2024). https://doi.org/10.1088/1361-6560/ad2e6a
60. M.K. Kozani, A. Magiera, Machine learning-based event recognition in SiFi compton camera imaging for proton therapy monitoring. Phys. Med. Biol. **67**(15), 155012 (2022). https://doi.org/10.1088/1361-6560/ac71f2
61. A.C. Kraan, Range verification methods in particle therapy: Underlying physics and monte carlo modeling. Front. Oncol. **5**, 150 (2015). https://doi.org/10.3389/fonc.2015.00150
62. G. Kraft, Tumor therapy with heavy charged particles. Prog. Part. Nucl. Phys. **45**, 473–544 (2000). https://doi.org/10.1016/S0146-6410(00)00112-5
63. J. Krimmer, M. Chevallier, J. Constanzo, D. Dauvergne, M.D. Rydt, G. Dedes, N. Freud, P. Henriquet, C.L. Tessa, J.M. Létang, R. Pleskač, M. Pinto, C. Ray, V. Reithinger, M.H. Richard, I. Rinaldi, F. Roellinghoff, C. Schuy, E. Testa, M. Testa, Collimated prompt gamma TOF measurements with multi-slit multi-detector configurations. J. Instrum. **10**(01), 01011 (2015). https://doi.org/10.1088/1748-0221/10/01/P01011
64. J. Krimmer, G. Angellier, L. Balleyguier, D. Dauvergne, N. Freud, J. Hérault, J.M. Létang, H. Mathez, M. Pinto, E. Testa, Y. Zoccarato, A cost-effective monitoring technique in particle therapy via uncollimated prompt gamma peak integration. Appl. Phys. Lett. **110**(15), 154102 (2017). https://doi.org/10.1063/1.4980103
65. J. Krimmer, D. Dauvergne, J.M.L. Etang, E. Testa, Prompt-gamma monitoring in hadrontherapy: a review. Nucl. Instrum. Methods Phys. Res., Sect. A **878**, 58–73 (2018). https://doi.org/10.1016/j.nima.2017.07.063. (**Radiation Imaging Techniques and Applications**)
66. Y. Ku, S. Choi, J. Cho, S. Jang, J.H. Jeong, S.H. Kim, S. Cho, C.H. Kim, Tackling range uncertainty in proton therapy: development and evaluation of a new multi-slit prompt-gamma camera (mspgc) system. Nucl. Eng. Technol. **55**(9), 3140–3149 (2023). https://doi.org/10.1016/j.net.2023.05.028
67. S. Kurosawa, H. Kubo, K. Ueno, S. Kabuki, S. Iwaki, M. Takahashi, K. Taniue, N. Higashi, K. Miuchi, T. Tanimori, D. Kim, J. Kim, Prompt gamma detection for range verification in proton therapy. Curr. Appl. Phys. **12**(2), 364–368 (2012). https://doi.org/10.1016/j.cap.2011.07.027
68. F. Lagerwaard, O. Bohoudi, S. Tetar, M.A. Admiraal, T.S. Rosario, A. Bruynzeel, Combined inter- and intrafractional plan adaptation using fraction partitioning in magnetic resonance-guided radiotherapy delivery. Cureus (2018). https://doi.org/10.7759/cureus.2434
69. F. Le Foulher, M. Bajard, M. Chevallier, D. Dauvergne, N. Freud, P. Henriquet, S. Karkar, J.M. Letang, L. Lestand, R. Plescak, C. Ray, D. Schardt, E. Testa, M. Testa, Monte carlo simulations of prompt-gamma emission during carbon ion irradiation. IEEE Trans. Nucl. Sci. **57**(5), 2768–2772 (2010). https://doi.org/10.1109/TNS.2010.2048042
70. J. Lerendegui-Marco, J. Balibrea-Correa, V. Babiano-Suárez, L. Caballero, C. Domingo-Pardo, I. Ladarescu, Simultaneous neutron and gamma imaging system for real time range and dose monitoring in hadron therapy and nuclear security applications. EPJ Web Conf. **261**, 05001 (2022). https://doi.org/10.1051/epjconf/202226105001
71. J. Lerendegui-Marco, J. Balibrea-Correa, V. Babiano-Suárez, I. Ladarescu, C. Domingo-Pardo, Towards machine learning aided real-time range imaging in proton therapy. Sci. Rep. **12**(1), 2735 (2022)
72. Z. Li, Y. Wang, Y. Yu, K. Fan, L. Xing, H. Peng, Technical note: Machine learning approaches for range and dose verification in proton therapy using proton-induced positron emitters. Med. Phys. **46**(12), 5748–5757 (2019). https://doi.org/10.1002/mp.13827
73. S. Lim-Reinders, B.M. Keller, S. Al-Ward, A. Sahgal, A. Kim, Online adaptive radiation therapy. Int. J. Radiat. Oncol. *Biol. *Phys. **99**(4), 994–1003 (2017). https://doi.org/10.1016/j.ijrobp.2017.04.023

74. C.-C. Liu, H.-M. Huang, A deep learning approach for converting prompt gamma images to proton dose distributions: a Monte Carlo simulation study. Phys. Med. **69**, 110–119 (2020). https://doi.org/10.1016/j.ejmp.2019.12.006
75. C. Liu, Z. Li, W. Hu, L. Xing, H. Peng, Range and dose verification in proton therapy using proton-induced positron emitters and recurrent neural networks (rnns). Phys. Med. Biol. **64**(17), 175009 (2019). https://doi.org/10.1088/1361-6560/ab3564
76. G. Llosá, J. Cabello, S. Callier, J.E. Gillam, C. Lacasta, M. Rafecas, L. Raux, C. Solaz, V. Stankova, C. de La Taille, M. Trovato, J. Barrio, First compton telescope prototype based on continuous labr3-sipm detectors. Nucl. Instrum. Methods Phys. Res., Sect. A **718**, 130–133 (2013). https://doi.org/10.1016/j.nima.2012.08.074. (**Proceedings of the 12th Pisa Meeting on Advanced Detectors**)
77. G. Llosá, M. Trovato, J. Barrio, A. Etxebeste, E. Muñoz, C. Lacasta, J.F. Oliver, M. Rafecas, C. Solaz, P. Solevi, First images of a three-layer compton telescope prototype for treatment monitoring in hadron therapy. Front. Oncol. (2016). https://doi.org/10.3389/fonc.2016.00014
78. A.J. Lomax, Myths and realities of range uncertainty. Br. J. Radiol. **93**(1107), 20190582 (2020). https://doi.org/10.1259/bjr.20190582
79. F.K. Longarino, T. Tessonnier, S. Mein, S.B. Harrabi, J. Debus, W. Stiller, A. Mairani, Dual-layer spectral ct for proton, helium, and carbon ion beam therapy planning of brain tumors. J. Appl. Clin. Med. Phys. **23**(1), 13465 (2022). https://doi.org/10.1002/acm2.13465
80. P.C. Lopes, E. Clementel, P. Crespo, S. Henrotin, J. Huizenga, G. Janssens, K. Parodi, D. Prieels, F. Roellinghoff, J. Smeets, F. Stichelbaut, D.R. Schaart, Time-resolved imaging of prompt-gamma rays for proton range verification using a knife-edge slit camera based on digital photon counters. Phys. Med. Biol. **60**(15), 6063 (2015). https://doi.org/10.1088/0031-9155/60/15/6063
81. P. Lysakovski, J. Besuglow, B. Kopp, S. Mein, T. Tessonnier, A. Ferrari, T. Haberer, J. Debus, A. Mairani, Development and benchmarking of the first fast monte carlo engine for helium ion beam dose calculation: monteray. Med. Phys. **50**(4), 2510–2524 (2023). https://doi.org/10.1002/mp.16178
82. J. Ma, C. Beltran, H. Seum Wan Chan Tseung, M.G. Herman, A GPU-accelerated and monte carlo-based intensity modulated proton therapy optimization system. Med. Phys. **41**(12), 121707 (2014). https://doi.org/10.1118/1.4901522
83. S. Ma, Z. Hu, K. Ye, X. Zhang, Y. Wang, H. Peng, Feasibility study of patient-specific dose verification in proton therapy utilizing positron emission tomography (pet) and generative adversarial network (gan). Med. Phys. **47**(10), 5194–5208 (2020). https://doi.org/10.1002/mp.14443
84. P. Magalhaes Martins, R. Dal Bello, B. Ackermann, S. Brons, G. Hermann, T. Kihm, J. Seco, PIBS: Proton and ion beam spectroscopy for in vivo measurements of oxygen, carbon, and calcium concentrations in the human body. Sci. Rep. **10**(1), 7007 (2020). https://doi.org/10.1038/s41598-020-63215-0
85. P. Magalhaes Martins, H. Freitas, T. Tessonnier, B. Ackermann, S. Brons, J. Seco, Towards real-time PGS range monitoring in proton therapy of prostate cancer. Sci. Rep. **11**(1), 15331 (2021). https://doi.org/10.1038/s41598-021-93612-y. (**Accessed 2024-02-09**)
86. A. Mairani, T.T. Böhlen, A. Schiavi, T. Tessonnier, S. Molinelli, S. Brons, G. Battistoni, K. Parodi, V. Patera, A monte carlo-based treatment planning tool for proton therapy. Phys. Med. Biol. **58**(8), 2471 (2013). https://doi.org/10.1088/0031-9155/58/8/2471
87. E. Malekzadeh, H. Rajabi, M.A. Tajik-Mansoury, P. Sabouri, E. Fiorina, F. Kalantari, Design and performance evaluation of a slit-slat camera for 2D prompt gamma imaging in proton therapy monitoring: A monte carlo simulation study. Med. Phys. **50**(6), 3701–3718 (2023). https://doi.org/10.1002/mp.16259
88. S. Marcatili, J. Collot, S. Curtoni, D. Dauvergne, J.-Y. Hostachy, C. Koumeir, J.M. Létang, J. Livingstone, V. Métivier, L. Gallin-Martel, M.L. Gallin-Martel, J.F. Muraz, N. Servagent, E. Testa, M. Yamouni, Ultra-fast prompt gamma detection in single proton counting regime for range monitoring in particle therapy. Phys. Med. Biol. **65**(24), 245033 (2020). https://doi.org/10.1088/1361-6560/ab7a6c
89. V. Mares, M. Romero-Expósito, J. Farah, S. Trinkl, C. Domingo, M. Dommert, L. Stolarczyk, L.V. Ryckeghem, M. Wielunski, P. Olko, R.M. Harrison, A comprehensive spectrometry study of a stray neutron radiation field in scanning proton therapy. Phys. Med. Biol. **61**(11), 4127 (2016). https://doi.org/10.1088/0031-9155/61/11/4127
90. T. Masuda, T. Nishio, J. Kataoka, M. Arimoto, A. Sano, K. Karasawa, ML-EM algorithm for dose estimation using PET in proton therapy. Phys. Med. Biol. **64**(17), 175011 (2019). https://doi.org/10.1088/1361-6560/ab3276
91. M. McCleskey, W. Kaye, D.S. Mackin, S. Beddar, Z. He, J.C. Polf, Evaluation of a multistage CdZnTe compton camera for prompt γ imaging for proton therapy. Nucl. Instrum. Methods Phys. Res., Sect. A **785**, 163–169 (2015). https://doi.org/10.1016/j.nima.2015.02.030
92. I. Meric, E. Alagoz, L.B. Hysing, T. Kögler, D. Lathouwers, W.R.B. Lionheart, J. Mattingly, J. Obhodas, G. Pausch, H.E.S. Pettersen, H.N. Ratliff, M. Rovituso, S.M. Schellhammer, L.M. Setterdahl, K. Skjerdal, E. Sterpin, D. Sudac, J.A. Turko, K.S. Ytre-Hauge, A hybrid multi-particle approach to range assessment-based treatment verification in particle therapy. Sci. Rep. **13**(1), 6709 (2023). https://doi.org/10.1038/s41598-023-33777-w
93. C.-H. Min, C.H. Kim, M.-Y. Youn, J.-W. Kim, Prompt gamma measurements for locating the dose falloff region in the proton therapy. Appl. Phys. Lett. **89**(18), 183517 (2006). https://doi.org/10.1063/1.2378561
94. C.H. Min, H.R. Lee, C.H. Kim, S.B. Lee, Development of array-type prompt gamma measurement system for in vivo range verification in proton therapy. Med. Phys. **39**(4), 2100–2107 (2012). https://doi.org/10.1118/1.3694098
95. H. Mizuno, T. Tomitani, M. Kanazawa, A. Kitagawa, J. Pawelke, Y. Iseki, E. Urakabe, M. Suda, A. Kawano, R. Iritani, S. Matsushita, T. Inaniwa, T. Nishio, S. Furukawa, K. Ando, Y.K. Nakamura, T. Kanai, K. Ishii, Washout measurement of radioisotope implanted by radioactive beams in the rabbit. Phys. Med. Biol. **48**(15), 2269 (2003). https://doi.org/10.1088/0031-9155/48/15/302
96. M. Moteabbed, S.E. Na, H. Paganetti, Monte Carlo patient study on the comparison of prompt gamma and PET imaging for range verification in proton therapy. Phys. Med. Biol. **56**(4), 1063 (2011). https://doi.org/10.1088/0031-9155/56/4/012
97. M. Moteabbed, A. Trofimov, G.C. Sharp, Y. Wang, A.L. Zietman, J.A. Efstathiou, H.-M. Lu, Proton therapy of prostate cancer by anterior-oblique beams: implications of setup and anatomy variations. Phys. Med. Biol. **62**(5), 1644 (2017). https://doi.org/10.1088/1361-6560/62/5/1644
98. S. Muraro, G. Battistoni, F. Collamati, E. De Lucia, R. Faccini, F. Ferroni, S. Fiore, P. Fralliccardi, M. Marafini, I. Mattei, S. Morganti, R. Paramatti, L. Piersanti, D. Pinci, A. Rucinski, A. Russomando, A. Sarti, A. Sciubba, E. Solfaroli-Camillocci, M. Toppi, G. Traini, C. Voena, V. Patera, Monitoring of hadrontherapy treatments by means of charged particle detection. Front. Oncol. **6**, 177 (2016). https://doi.org/10.3389/fonc.2016.00177
99. L. Nenoff, M. Matter, M. Charmillot, S. Krier, K. Uher, D.C. Weber, A.J. Lomax, F. Albertini, Experimental validation of daily adaptive proton therapy. Phys. Med. Biol. **66**(20), 205010 (2021). https://doi.org/10.1088/1361-6560/ac2b84
100. W.D. Newhauser, R. Zhang, The physics of proton therapy. Phys. Med. Biol. **60**(8), 155 (2015). https://doi.org/10.1088/0031-9155/60/8/R155
101. K.R. Padgett, G. Simpson, D. Asher, L. Portelance, E. Bossart, N. Dogan, Assessment of online adaptive MR-guided stereotactic body radiotherapy of liver cancers. Phys. Med. **77**, 54–63 (2020). https://doi.org/10.1016/j.ejmp.2020.07.027
102. H. Paganetti, Range uncertainties in proton therapy and the role of monte carlo simulations. Phys. Med. Biol. **57**(11), 99 (2012). https://doi.org/10.1088/0031-9155/57/11/R99
103. H. Paganetti, G. El Fakhri, Monitoring proton therapy with pet. Br. J. Radiol. **88**(1051), 20150173 (2015). https://doi.org/10.1259/bjr.20150173. (**PMID: 25989699**)
104. H. Paganetti, P. Botas, G.C. Sharp, B. Winey, Adaptive proton therapy. Phys. Med. Biol. **66**(22), 22 (2021). https://doi.org/10.1088/1361-6560/ac344f
105. R. Panthi, P. Maggi, S. Peterson, D. Mackin, J. Polf, S. Beddar, Secondary particle interactions in a compton camera designed for in vivo range verification of proton therapy. IEEE Trans. Radiat. Plasma Med. Sci. **5**(3), 383–391 (2021). https://doi.org/10.1109/TRPMS.2020.3030166

106. J.H. Park, S.H. Kim, Y. Ku, C.H. Kim, H.R. Lee, J.H. Jeong, S.B. Lee, D.H. Shin, Multi-slit prompt-gamma camera for locating of distal dose falloff in proton therapy. Nucl. Eng. Technol. **51**(5), 1406–1416 (2019). https://doi.org/10.1016/j.net.2019.03.008
107. K. Parodi, T. Bortfeld, A filtering approach based on gaussian-powerlaw convolutions for local PET verification of proton radiotherapy. Phys. Med. Biol. **51**(8), 1991 (2006). https://doi.org/10.1088/0031-9155/51/8/003
108. K. Parodi, W. Enghardt, Potential application of PET in quality assurance of proton therapy. Phys. Med. Biol. **45**(11), 151 (2000). https://doi.org/10.1088/0031-9155/45/11/403
109. K. Parodi, W. Enghardt, T. Haberer, In-beam pet measurements of β+ radioactivity induced by proton beams. Phys. Med. Biol. **47**(1), 21 (2001). https://doi.org/10.1088/0031-9155/47/1/302
110. K. Parodi, H. Paganetti, H.A. Shih, S. Michaud, J.S. Loeffler, T.F. DeLaney, N.J. Liebsch, J.E. Munzenrider, A.J. Fischman, A. Knopf, T. Bortfeld, Patient study of in vivo verification of beam delivery and range, using positron emission tomography and computed tomography imaging after proton therapy. Int. J. Radiat. Oncol. *Biol. *Phys. **68**(3), 920–934 (2007). https://doi.org/10.1016/j.ijrobp.2007.01.063
111. F. Pennazio, V. Ferrero, G. D'Onghia, S. Garbolino, E. Fiorina, O.A.M. Villarreal, F.M. Milian, V. Monaco, V. Monti, A. Patera, J. Werner, R. Wheadon, M. Rafecas, Proton therapy monitoring: spatiotemporal emission reconstruction with prompt gamma timing and implementation with PET detectors. Phys. Med. Biol. **67**(6), 065005 (2022). https://doi.org/10.1088/1361-6560/ac5765
112. I. Perali, A. Celani, L. Bombelli, C. Fiorini, F. Camera, E. Clementel, S. Henrotin, G. Janssens, D. Prieels, F. Roellinghoff, J. Smeets, F. Stichelbaut, F.V. Stappen, Prompt gamma imaging of proton pencil beams at clinical dose rate. Phys. Med. Biol. **59**(19), 5849 (2014). https://doi.org/10.1088/0031-9155/59/19/5849
113. J. Perl, J. Shin, J. Schümann, B. Faddegon, H. Paganetti, TOPAS: an innovative proton monte carlo platform for research and clinical applications. Med. Phys. **39**(11), 6818–6837 (2012). https://doi.org/10.1118/1.4758060
114. S.W. Peterson, D. Robertson, J. Polf, Optimizing a three-stage compton camera for measuring prompt gamma rays emitted during proton radiotherapy. Phys. Med. Biol. **55**(22), 6841 (2010). https://doi.org/10.1088/0031-9155/55/22/015
115. D. Pflugfelder, J.J. Wilkens, U. Oelfke, Worst case optimization: a method to account for uncertainties in the optimization of intensity modulated proton therapy. Phys. Med. Biol. **53**(6), 1689 (2008). https://doi.org/10.1088/0031-9155/53/6/013
116. J. Pietsch, C. Khamfongkhruea, J. Berthold, G. Janssens, K. Stützer, S. Löck, C. Richter, Automatic detection and classification of treatment deviations in proton therapy from realistically simulated prompt gamma imaging data. Med. Phys. **50**(1), 506–517 (2023). https://doi.org/10.1002/mp.15975
117. M. Pinto, M. Bajard, S. Brons, M. Chevallier, D. Dauvergne, G. Dedes, M.D. Rydt, N. Freud, J. Krimmer, C.L. Tessa, J.M. Létang, K. Parodi, R. Pleskač, D. Prieels, C. Ray, I. Rinaldi, F. Roellinghoff, D. Schardt, E. Testa, M. Testa, Absolute prompt-gamma yield measurements for ion beam therapy monitoring. Phys. Med. Biol. **60**(2), 565 (2014). https://doi.org/10.1088/0031-9155/60/2/565
118. M. Pinto, D. Dauvergne, N. Freud, J. Krimmer, J.M. Letang, C. Ray, F. Roellinghoff, E. Testa, Design optimisation of a TOF-based collimated camera prototype for online hadrontherapy monitoring. Phys. Med. Biol. **59**(24), 7653 (2014). https://doi.org/10.1088/0031-9155/59/24/7653
119. M. Pinto, D. Dauvergne, N. Freud, J. Krimmer, J.M. Létang, E. Testa, Assessment of Geant4 prompt-gamma emission yields in the context of proton therapy monitoring. Front. Oncol. (2016). https://doi.org/10.3389/fonc.2016.00010
120. M. Pinto, K. Kröniger, J. Bauer, R. Nilsson, E. Traneus, K. Parodi, A filtering approach for PET and PG predictions in a proton treatment planning system. Phys. Med. Biol. **65**(9), 095014 (2020). https://doi.org/10.1088/1361-6560/ab8146
121. J.C. Polf, S. Peterson, G. Ciangaru, M. Gillin, S. Beddar, Prompt gamma-ray emission from biological tissues during proton irradiation: a preliminary study. Phys. Med. Biol. **54**(3), 731 (2009). https://doi.org/10.1088/0031-9155/54/3/017
122. J.C. Polf, S. Peterson, M. McCleskey, B.T. Roeder, A. Spiridon, S. Beddar, L. Trache, Measurement and calculation of characteristic prompt gamma ray spectra emitted during proton irradiation. Phys. Med. Biol. **54**(22), 519 (2009). https://doi.org/10.1088/0031-9155/54/22/N02
123. J.C. Polf, S. Avery, D.S. Mackin, S. Beddar, Imaging of prompt gamma rays emitted during delivery of clinical proton beams with a compton camera: feasibility studies for range verification. Phys. Med. Biol. **60**(18), 7085 (2015). https://doi.org/10.1088/0031-9155/60/18/7085
124. J.C. Polf, C.A. Barajas, S.W. Peterson, D.S. Mackin, S. Beddar, L. Ren, M.K. Gobbert, Applications of machine learning to improve the clinical viability of Compton camera based in vivo range verification in proton radiotherapy. Front. Phys. (2022). https://doi.org/10.3389/fphy.2022.838273
125. G. Poludniowski, N.M. Allinson, P.M. Evans, Proton radiography and tomography with application to proton therapy. Br. J. Radiol. **88**(1053), 20150134 (2015). https://doi.org/10.1259/bjr.20150134
126. P.G. Prasanna, K. Rawojc, C. Guha, J.C. Buchsbaum, J.U. Miszczyk, C.N. Coleman, Normal tissue injury induced by photon and proton therapies: gaps and opportunities. Int. J. Radiat. Oncol. *Biol. *Phys. **110**(5), 1325–1340 (2021). https://doi.org/10.1016/j.ijrobp.2021.02.043
127. M. Priegnitz, S. Helmbrecht, G. Janssens, I. Perali, J. Smeets, F.V. Stappen, E. Sterpin, F. Fiedler, Measurement of prompt gamma profiles in inhomogeneous targets with a knife-edge slit camera during proton irradiation. Phys. Med. Biol. **60**(12), 4849 (2015). https://doi.org/10.1088/0031-9155/60/12/4849
128. M. Priegnitz, S. Helmbrecht, G. Janssens, I. Perali, J. Smeets, F.V. Stappen, E. Sterpin, F. Fiedler, Detection of mixed-range proton pencil beams with a prompt gamma slit camera. Phys. Med. Biol. **61**(2), 855 (2016). https://doi.org/10.1088/0031-9155/61/2/855
129. M. Priegnitz, S. Barczyk, L. Nenoff, C. Golnik, I. Keitz, T. Werner, S. Mein, J. Smeets, F.V. Stappen, G. Janssens, L. Hotoiu, F. Fiedler, D. Prieels, W. Enghardt, G. Pausch, C. Richter, Towards clinical application: prompt gamma imaging of passively scattered proton fields with a knife-edge slit camera. Phys. Med. Biol. **61**(22), 7881 (2016). https://doi.org/10.1088/0031-9155/61/22/7881
130. N. Qin, M. Pinto, Z. Tian, G. Dedes, A. Pompos, S.B. Jiang, K. Parodi, X. Jia, Initial development of goCMC: a GPU-oriented fast cross-platform Monte Carlo engine for carbon ion therapy. Phys. Med. Biol. **62**(9), 3682 (2017). https://doi.org/10.1088/1361-6560/aa5d43
131. S. Remmele, J. Hesser, H. Paganetti, T. Bortfeld, A deconvolution approach for PET-based dose reconstruction in proton radiotherapy. Phys. Med. Biol. **56**(23), 7601 (2011). https://doi.org/10.1088/0031-9155/56/23/017
132. M.-H. Richard, M. Chevallier, D. Dauvergne, N. Freud, P. Henriquet, F. Le Foulher, J.M. Létang, G. Montarou, C. Ray, F. Roellinghoff, E. Testa, M. Testa, A.H. Walenta, Design study of a compton camera for prompt γ imaging during ion beam therapy. In: 2009 IEEE Nuclear Science Symposium Conference Record (NSS/MIC), pp 4172–4175 (2009). https://doi.org/10.1109/NSSMIC.2009.5402293
133. M.-H. Richard, M. Chevallier, D. Dauvergne, N. Freud, P. Henriquet, F. Le Foulher, J.M. Létang, G. Montarou, C. Ray, F. Roellinghoff, E. Testa, M. Testa, A.H. Walenta, Design guidelines for a double scattering compton camera for prompt-γ imaging during ion beam therapy: A monte carlo simulation study. IEEE Trans. Nucl. Sci. **58**(1), 87–94 (2011). https://doi.org/10.1109/TNS.2010.2076303
134. C. Richter, G. Pausch, S. Barczyk, M. Priegnitz, I. Keitz, J. Thiele, J. Smeets, F.V. Stappen, L. Bombelli, C. Fiorini, L. Hotoiu, I. Perali, D. Prieels, W. Enghardt, M. Baumann, First clinical application of a prompt gamma based in vivo proton range verification system. Radiother. Oncol. **118**(2), 232–237 (2016). https://doi.org/10.1016/j.radonc.2016.01.004
135. M.E. Rising, J.C. Armstrong, S.R. Bolding, F.B. Brown, J.S. Bull, T.P. Burke, A.R. Clark, D.A. Dixon, R.A. Forster, III, J.F. Giron, T.S. Grieve, H.G. Hughes, III, C.J. Josey, J.A. Kulesza, R.L. Martz, A.P. McCartney, G.W. McKinney, S.W. Mosher, E.J. Pearson, C.J. Solomon, Jr., S. Swaminarayan, J.E. Sweezy, S.C. Wilson, A.J. Zukaitis, MCNP® Code Version 6.3.0 Release Notes. Technical Report LA-UR-22-33103, Rev. 1, Los Alamos National Laboratory, Los Alamos, NM, USA (January 2023). https://doi.org/10.2172/1909545. https://www.osti.gov/biblio/1909545

136. F. Roellinghoff, M.-H. Richard, M. Chevallier, J. Constanzo, D. Dauvergne, N. Freud, P. Henriquet, F. Le Foulher, J.M. Létang, G. Montarou, C. Ray, E. Testa, M. Testa, A.H. Walenta, Design of a compton camera for 3d prompt-γ imaging during ion beam therapy. Nucl. Instrum. Methods Phys. Res., Sect. A **648**, 20–23 (2011). https://doi.org/10.1016/j.nima.2011.01.069
137. F. Roellinghoff, A. Benilov, D. Dauvergne, G. Dedes, N. Freud, G. Janssens, J. Krimmer, J.M. Létang, M. Pinto, D. Prieels, C. Ray, J. Smeets, F. Stichelbaut, E. Testa, Real-time proton beam range monitoring by means of prompt-gamma detection with a collimated camera. Phys. Med. Biol. **59**(5), 1327 (2014). https://doi.org/10.1088/0031-9155/59/5/1327
138. K. Roemer, G. Pausch, D. Bemmerer, M. Berthel, A. Dreyer, C. Golnik, F. Hueso-González, T. Kormoll, J. Petzoldt, H. Rohling, P. Thirolf, A. Wagner, L. Wagner, D. Weinberger, F. Fiedler, Characterization of scintillator crystals for usage as prompt gamma monitors in particle therapy. J. Instrum. **10**(10), 10033 (2015). https://doi.org/10.1088/1748-0221/10/10/P10033
139. A. Rucinski, G. Battistoni, F. Collamati, E.D. Lucia, R. Faccini, P.M. Frallicciardi, C. Mancini-Terracciano, M. Marafini, I. Mattei, S. Muraro, R. Paramatti, L. Piersanti, D. Pinci, A. Russomando, A. Sarti, A. Sciubba, E.S. Camillocci, M. Toppi, G. Traini, C. Voena, V. Patera, Secondary radiation measurements for particle therapy applications: charged particles produced by 4He and 12C ion beams in a PMMA target at large angle. Phys. Med. Biol. **63**(5), 055018 (2018). https://doi.org/10.1088/1361-6560/aaa36a
140. H. Rutherford, A. Chacon, A. Mohammadi, S. Takyu, H. Tashima, E. Yoshida, F. Nishikido, T. Hofmann, M. Pinto, D.R. Franklin, T. Yamaya, K. Parodi, A.B. Rosenfeld, S. Guatelli, M. Safavi-Naeini, Dose quantification in carbon ion therapy using in-beam positron emission tomography. Phys. Med. Biol. **65**(23), 235052 (2020). https://doi.org/10.1088/1361-6560/abaa23
141. M. Sakai, S. Tamaki, I. Murata, R.K. Parajuli, A. Matsumura, N. Kubo, M. Tashiro, Experimental study on Compton camera for boron neutron capture therapy applications. Sci. Rep. **13**(1), 22883 (2023). https://doi.org/10.1038/s41598-023-49955-9
142. S.M. Schellhammer, S. Gantz, A. Lühr, B.M. Oborn, M. Bussmann, A.L. Hoffmann, Technical note: experimental verification of magnetic field-induced beam deflection and Bragg peak displacement for MR-integrated proton therapy. Med. Phys. **45**(7), 3429–3434 (2018). https://doi.org/10.1002/mp.12961
143. A. Schiavi, M. Senzacqua, S. Pioli, A. Mairani, G. Magro, S. Molinelli, M. Ciocca, G. Battistoni, V. Patera, Fred: a GPU-accelerated fast-Monte Carlo code for rapid treatment plan recalculation in ion beam therapy. Phys. Med. Biol. **62**(18), 7482 (2017). https://doi.org/10.1088/1361-6560/aa8134
144. R.W. Schulte, V. Bashkirov, M.C. Loss Klock, T. Li, A.J. Wroe, I. Evseev, D.C. Williams, T. Satogata, Density resolution of proton computed tomography. Med. Phys. **32**(4), 1035–1046 (2005). https://doi.org/10.1118/1.1884906
145. A. Schumann, J. Petzoldt, P. Dendooven, W. Enghardt, C. Golnik, F. Hueso-González, T. Kormoll, G. Pausch, K. Roemer, F. Fiedler, Simulation and experimental verification of prompt gamma-ray emissions during proton irradiation. Phys. Med. Biol. **60**(10), 4197 (2015). https://doi.org/10.1088/0031-9155/60/10/4197
146. A. Schumann, M. Priegnitz, S. Schoene, W. Enghardt, H. Rohling, F. Fiedler, From prompt gamma distribution to dose: a novel approach combining an evolutionary algorithm and filtering based on gaussian-powerlaw convolutions. Phys. Med. Biol. **61**(19), 6919–6934 (2016). https://doi.org/10.1088/0031-9155/61/19/6919
147. G. Shakirin, H. Braess, F. Fiedler, D. Kunath, K. Laube, K. Parodi, M. Priegnitz, W. Enghardt, Implementation and workflow for PET monitoring of therapeutic ion irradiation: a comparison of in-beam, in-room, and off-line techniques. Phys. Med. Biol. **56**(5), 1281 (2011). https://doi.org/10.1088/0031-9155/56/5/004
148. S. Shimizu, K. Nishioka, R. Suzuki, N. Shinohara, S. Maruyama, T. Abe, R. Kinoshita, N. Katoh, R. Onimaru, H. Shirato, Early results of urethral dose reduction and small safety margin in intensity-modulated radiation therapy (IMRT) for localized prostate cancer using a real-time tumor-tracking radiotherapy (RTRT) system. Radiat. Oncol. **9**(1), 118 (2014)
149. J. Smeets, F. Roellinghoff, D. Prieels, F. Stichelbaut, A. Benilov, P. Busca, C. Fiorini, R. Peloso, M. Basilavecchia, T. Frizzi, J.C. Dehaes, A. Dubus, Prompt gamma imaging with a slit camera for real-time range control in proton therapy. Phys. Med. Biol. **57**(11), 3371 (2012). https://doi.org/10.1088/0031-9155/57/11/3371
150. J. Smeets, F. Roellinghoff, G. Janssens, I. Perali, A. Celani, C. Fiorini, N. Freud, E. Testa, D. Prieels, Experimental comparison of knife-edge and multi-parallel slit collimators for prompt gamma imaging of proton pencil beams. Front. Oncol. **6**, 156 (2016). https://doi.org/10.3389/fonc.2016.00156
151. K. Souris, J.A. Lee, E. Sterpin, Fast multipurpose monte carlo simulation for proton therapy using multi- and many-core cpu architectures. Med. Phys. **43**(4), 1700–1712 (2016). https://doi.org/10.1118/1.4943377
152. K. Souris, A. Barragan Montero, G. Janssens, D. Di Perri, E. Sterpin, J.A. Lee, Technical note: Monte carlo methods to comprehensively evaluate the robustness of 4d treatments in proton therapy. Med. Phys. **46**(10), 4676–4684 (2019). https://doi.org/10.1002/mp.13749
153. E. Sterpin, J. Sorriaux, S. Vynckier, Extension of penelope to protons: simulation of nuclear reactions and benchmark with geant4. Med. Phys. **40**(11), 111705 (2013). https://doi.org/10.1118/1.4823469
154. E. Sterpin, G. Janssens, J. Smeets, F.V. Stappen, D. Prieels, M. Priegnitz, I. Perali, S. Vynckier, Analytical computation of prompt gamma ray emission and detection for proton range verification. Phys. Med. Biol. **60**(12), 4915 (2015). https://doi.org/10.1088/0031-9155/60/12/4915
155. S. Sun, Y. Liu, X. Ouyang, Design and performance evaluation of a coded aperture imaging system for real-time prompt gamma-ray monitoring during proton therapy. Radiat. Phys. Chem. **174**, 108891 (2020). https://doi.org/10.1016/j.radphyschem.2020.108891
156. S. Tanaka, N. Miyamoto, Y. Matsuo, T. Yoshimura, S. Takao, T. Matsuura, First experimental results of gated proton imaging using x-ray fluoroscopy to detect a fiducial marker. Phys. Med. Biol. **66**(18), 18 (2021). https://doi.org/10.1088/1361-6560/ac212b
157. S. Tang, S. Both, H. Bentefour, J.J. Paly, Z. Tochner, J. Efstathiou, H.-M. Lu, Improvement of prostate treatment by anterior proton fields. Int. J. Radiat. Oncol. *Biol. *Phys. **83**(1), 408–418 (2012). https://doi.org/10.1016/j.ijrobp.2011.06.1974
158. S. Tattenberg, T.M. Madden, T. Bortfeld, K. Parodi, J. Verburg, Range uncertainty reductions in proton therapy may lead to the feasibility of novel beam arrangements which improve organ-at-risk sparing. Med. Phys. **49**(7), 4693–4704 (2022). https://doi.org/10.1002/mp.15644
159. S. Tattenberg, R. Marants, K. Niepel, T. Bortfeld, A. Sudhyadhom, G. Landry, K. Parodi, J. Verburg, Validation of prompt gamma-ray spectroscopy for proton range verification in tissue-mimicking and porcine samples. Phys. Med. Biol. **67**(20), 205006 (2022). https://doi.org/10.1088/1361-6560/ac950f
160. E. Testa, M. Bajard, M. Chevallier, D. Dauvergne, F. Le Foulher, N. Freud, J.-M. Létang, J.-C. Poizat, C. Ray, M. Testa, Monitoring the bragg peak location of 73 MeV/u carbon ions by means of prompt γ-ray measurements. Appl. Phys. Lett. **93**(9), 093506 (2008). https://doi.org/10.1063/1.2975841
161. M. Testa, M. Bajard, M. Chevallier, D. Dauvergne, N. Freud, P. Henriquet, S. Karkar, F. Le Foulher, J.M. Létang, R. Plescak, C. Ray, M.-H. Richard, D. Schardt, E. Testa, Real-time monitoring of the Bragg-peak position in ion therapy by means of single photon detection. Radiat. Environ. Biophys. **49**(3), 337–343 (2010). https://doi.org/10.1007/s00411-010-0276-2
162. M. Testa, C.H. Min, J.M. Verburg, J. Schümann, H.-M. Lu, H. Paganetti, Range verification of passively scattered proton beams based on prompt gamma time patterns. Phys. Med. Biol. **59**(15), 4181 (2014). https://doi.org/10.1088/0031-9155/59/15/4181
163. P.G. Thirolf, C. Lang, S. Aldawood, H.G. Kolff, L. Maier, D.R. Schaart, K. Parodi, Development of a compton camera for online range monitoring of laser-accelerated proton beams via prompt-gamma detection. EPJ Web Conf. **66**, 11036 (2014). https://doi.org/10.1051/epjconf/20146611036

164. L. Tian, G. Landry, G. Dedes, F. Kamp, M. Pinto, K. Niepel, C. Belka, K. Parodi, Toward a new treatment planning approach accounting for in vivo proton range verification. Phys. Med. Biol. **63**(21), 215025 (2018). https://doi.org/10.1088/1361-6560/aae749
165. L. Tian, G. Landry, G. Dedes, M. Pinto, F. Kamp, C. Belka, K. Parodi, A new treatment planning approach accounting for prompt gamma range verification and interfractional anatomical changes. Phys. Med. Biol. **65**(9), 095005 (2020). https://doi.org/10.1088/1361-6560/ab7d15
166. L. Tian, Z. Huang, G. Janssens, G. Landry, G. Dedes, F. Kamp, C. Belka, M. Pinto, K. Parodi, Accounting for prompt gamma emission and detection for range verification in proton therapy treatment planning. Phys. Med. Biol. **66**(5), 055005 (2021). https://doi.org/10.1088/1361-6560/abc939
167. R.W. Todd, J.M. Nightingale, D.B. Everett, A proposed γ camera. Nature **251**(5471), 132–134 (1974). https://doi.org/10.1038/251132a0
168. J. Unkelbach, T.C.Y. Chan, T. Bortfeld, Accounting for range uncertainties in the optimization of intensity modulated proton therapy. Phys. Med. Biol. **52**(10), 2755 (2007). https://doi.org/10.1088/0031-9155/52/10/009
169. J.M. Verburg, J. Seco, Proton range verification through prompt gamma-ray spectroscopy. Phys. Med. Biol. **59**(23), 7089 (2014). https://doi.org/10.1088/0031-9155/59/23/7089
170. J.M. Verburg, H.A. Shih, J. Seco, Simulation of prompt gamma-ray emission during proton radiotherapy. Phys. Med. Biol. **57**(17), 5459 (2012). https://doi.org/10.1088/0031-9155/57/17/5459
171. J.M. Verburg, K. Riley, T. Bortfeld, J. Seco, Energy- and time-resolved detection of prompt gamma-rays for proton range verification. Phys. Med. Biol. **58**(20), 37 (2013). https://doi.org/10.1088/0031-9155/58/20/L37
172. J.M. Verburg, C. Grassberger, S. Dowdell, J. Schuemann, J. Seco, H. Paganetti, Automated monte carlo simulation of proton therapy treatment plans. Technol. Cancer Res. Treatment **15**(6), 35–46 (2016). https://doi.org/10.1177/1533034615614139. (**PMID: 26596915**)
173. V. Vlachoudis, FLAIR: A powerful but user friendly graphical interface for FLUKA. In: Int. Conf. on Mathematics, Computational Methods & Reactor Physics (M &C 2009) (2009)
174. H. Wan Chan Tseung, C. Beltran, A graphics processor-based intranuclear cascade and evaporation simulation. Comput. Phys. Commun. **185**(7), 2029–2033 (2014). https://doi.org/10.1016/j.cpc.2014.04.007
175. H. Wan Chan Tseung, J. Ma, C. Beltran, A fast gpu-based monte carlo simulation of proton transport with detailed modeling of nonelastic interactions. Med. Phys. **42**(6Part1), 2967–2978 (2015). https://doi.org/10.1118/1.4921046
176. T. Werner, J. Berthold, F. Hueso-González, T. Koegler, J. Petzoldt, K. Roemer, C. Richter, A. Rinscheid, A. Straessner, W. Enghardt, G. Pausch, Processing of prompt gamma-ray timing data for proton range measurements at a clinical beam delivery. Phys. Med. Biol. **64**(10), 105023 (2019). https://doi.org/10.1088/1361-6560/ab176d
177. A. Wrońska, J. Kasper, A.A. Ahmed, A. Andres, P. Bednarczyk, G. Gazdowicz, K. Herweg, R. Hetzel, A. Konefał, P. Kulessa, A. Magiera, K. Rusiecka, D. Stachura, A. Stahl, M. Ziebliński, Prompt-gamma emission in GEANT4 revisited and confronted with experiment. Phys. Med. **88**, 250–261 (2021). https://doi.org/10.1016/j.ejmp.2021.07.018
178. Y. Xie, E.H. Bentefour, G. Janssens, J. Smeets, F. Vander Stappen, L. Hotoiu, L. Yin, D. Dolney, S. Avery, F. O'Grady, D. Prieels, J. McDonough, T.D. Solberg, R.A. Lustig, A. Lin, B.-K.K. Teo, Prompt gamma imaging for in vivo range verification of pencil beam scanning proton therapy. Int. J. Radiat. Oncol. Biol. Phys. **99**(1), 210–218 (2017)
179. M. Yamaguchi, Y. Nagao, K. Ando, S. Yamamoto, T. Toshito, J. Kataoka, N. Kawachi, Secondary-electron-bremsstrahlung imaging for proton therapy. Nucl. Instrum. Methods Phys. Res., Sect. A **833**, 199–207 (2016). https://doi.org/10.1016/j.nima.2016.07.034
180. M. Yamaguchi, Y. Nagao, K. Ando, S. Yamamoto, M. Sakai, R.K. Parajuli, K. Arakawa, N. Kawachi, Imaging of monochromatic beams by measuring secondary electron bremsstrahlung for carbon-ion therapy using a pinhole x-ray camera. Phys. Med. Biol. **63**(4), 045016 (2018). https://doi.org/10.1088/1361-6560/aaa17c
181. D. Yan, F. Vicini, J. Wong, A. Martinez, Adaptive radiation therapy. Phys. Med. Biol. **42**(1), 123 (1997). https://doi.org/10.1088/0031-9155/42/1/008
182. K.S. Ytre-Hauge, K. Skjerdal, J. Mattingly, I. Meric, A Monte Carlo feasibility study for neutron based real-time range verification in proton therapy. Sci. Rep. (2011). https://doi.org/10.1038/s41598-019-38611-w
183. Y. Yuan, O.C. Andronesi, T.R. Bortfeld, C. Richter, R. Wolf, A.R. Guimaraes, T.S. Hong, J. Seco, Feasibility study of in vivo MRI based dosimetric verification of proton end-of-range for liver cancer patients. Radiother. Oncol. **106**(3), 378–382 (2013). https://doi.org/10.1016/j.radonc.2013.01.016
184. J. Zhang, Y. Lu, W. Hsi, J. Zhang, Y. Sheng, L. Shi, W. Wang, J. Lu, R. Zhou, J. Cheng, Evaluation of proton therapy accuracy using a PMMA phantom and PET prediction module. Front. Oncol. (2018). https://doi.org/10.3389/fonc.2018.00523
185. J. Zhang, Y. Lu, Y. Sheng, W. Wang, Z. Hong, Y. Sun, R. Zhou, J. Cheng, A comparative study of two in vivo PET verification methods in clinical cases. Front. Oncol. (2021). https://doi.org/10.3389/fonc.2021.617787